Topological entanglement entropy and gapless Majorana edge modes in the three-dimensional Kitaev model

A thesis submitted

in partial fulfillment for the award of the degree of

Doctor of Philosophy

in

Physics

by

Randeep N C

Department of Physics

Indian Institute of Space Science and Technology

Thiruvananthapuram, India

18 May 2020

Certificate

This is to certify that the thesis titled ***Topological entanglement entropy and gapless Majorana edge modes in the three-dimensional Kitaev model*** submitted by **Randeep N C**, to the Indian Institute of Space Science and Technology, Thiruvananthapuram, in partial fulfillment for the award of the degree of **Doctor of Philosophy** in **Physics**, is a bonafide record of the internship work carried out by him/her under my supervision. The contents of this report, in full or in parts, have not been submitted to any other Institute or University for the award of any degree or diploma.

Dr. Naveen Surendran
Associate Professor,
Department of Physics,
IIST, Thiruvananthapuram.

Dr. Umesh R. Kadhane
Associate Professor and Head,
Department of Physics,
IIST, Thiruvananthapuram.

Place: Thiruvananthapuram
Date: 18 May 2020

Declaration

I declare that this thesis titled ***Topological entanglement entropy and gapless Majorana edge modes in the three-dimensional Kitaev model*** submitted in partial fulfillment for the award of the degree of **Doctor of Philosophy** in **Physics** is a record of original work carried out by me under the supervision of **Dr. Naveen Surendran**, and has not formed the basis for the award of any degree, diploma, associateship, fellowship, or other titles in this or any other Institution or University of higher learning. In keeping with the ethical practice in reporting scientific information, due acknowledgments have been made wherever the findings of others have been cited.

Place: Thiruvananthapuram
Date: 18 May 2020

Randeep N C
(SC13D006)

This thesis is dedicated to my Parents...

Acknowledgements

I take this opportunity to express my sincere gratitude to my research supervisor, Dr. Naveen Surendran, without his assistance and dedicated involvement in every step throughout my Ph.D period, this thesis would have never been accomplished. I thank the members of my doctoral committee, Dr. C. S. Narayanamurthy, Dr. S. Murugesh, Dr. R. Shankar, Dr. Sreedhar B. Dutta and Dr. Anand Narayanan, for their guidance and support during annual reviews. I thank Dr. Umesh. R. Kadhane, the Head of the Department of Physics, Dr. C. S. Narayanamurthy and Dr. S. Murugesh former Heads of the Department of Physics and all other faculty members of the Physics department for creating such a stimulating environment conducive for fundamental research. It is my pleasure to thank the Director, Dr. Vinay Kumar Dadhwal, the former Director, Dr. K. S. Dasgupta. I thank IIST for financially supporting me during my Ph.D candidature with a generous fellowship.

I express my overwhelming gratitude to my parents and my sister for their love and support. I thank all my friends Sachin, Manjunath, Shiju, Rajesh Rajagopal, Deepak M, Deepak Gopalakrishnan, Praveen, Karthika, Soumya, Sarath and Dileep for their friendship and support. Last, but not least, I thank my partner Binsha E for her encouragement and support during most difficult periods of my Ph.D period.

Randeep N C

Abstract

In this thesis, we have studied two different topological aspects of the three-dimensional Kitaev model on hyperhoneycomb lattice, a generalization of Kitaev's honeycomb lattice spin model. In the first part we have calculated the topological entanglement entropy (TEE). We find that for this model TEE is not directly determined by the total quantum dimension of the system. This is in contrast to general two dimensional systems and many three dimensional models, where TEE is related to the total quantum dimension. Our calculation also provides TEE for a three-dimensional toric-code-type Hamiltonian that emerges as the effective low-energy theory for the Kitaev model in a particular limit.

In the second part we have obtained analytical solutions for the zero-energy Majorana edge modes. We have considered three types of edges—zigzag, bearded and armchair—and found the regions in parameter space where each type of edge mode exists. In the gapless phase, we obtain edge state solutions which are the drumhead surface states associated with nodal-line semimetals. We have also found a correspondence between noninteracting complex fermions and Majorana fermions on bipartite lattices, which explains the equivalence of energy spectrum and eigenmodes of Kitaev model and a corresponding tight-binding model for complex fermions on the same lattice.

Contents

List of Figures **xiii**

List of Tables **xv**

Abbreviations **xvii**

Nomenclature **xix**

1 Introduction **1**

1.1 Entanglement Entropy 2

1.2 Zero energy Majorana edge modes 7

1.3 Outline of the following chapters 7

2 The Kitaev Model **9**

2.1 Kitaev Hamiltonian 10

2.2 Three dimensional Kitaev Model 16

3 Topological Entanglement Entropy **20**

3.1 Entanglement entropy 21

3.2 Topological entanglement entropy 23

3.3 Summary 25

4 Zero Energy Majorana Edge Modes **27**

4.1 Bulk energy spectrum 28

4.2 Zero-energy edge modes 31

4.3 Correspondence between Majorana modes and fermion modes on bipartite lattices 39

4.4 Summary 42

5 Summary and Discussion **43**

Bibliography **44**

List of Publications **55**

Appendices **57**

A Entanglement entropy of the gauge sector **57**

B Existence condition for armchair edge modes **60**

List of Figures

1.1 Composite system with subsystems A and B 2

1.2 The plane is divided into four regions, labeled A, B, C and D (Kitaev and Preskill, 2006). 6

1.3 Different partitions considered in the Levin-Wen scheme. 6

2.1 Honeycomb lattice: the two sites labeled A(green) and B(red) belong to a unit cell; $\mathbf{v}_1$, and $\mathbf{v}_2$ are basis vectors; x, y and z are the link labels. Plaquette p consists of sites marked $1-6$. 10

2.2 Phase diagram on the plane $J_x + J_y + J_z = 1$. Region A is gapped and region B gapless. 14

2.3 Square lattice on the torus; s represents the star operator; p represents the plaquette operator. 15

2.4 The 3D lattice: the four sites labeled A(red), B(yellow), C(blue) and D(green) belong to a unit cell; a_1, a_2, a_3 are the basis vectors; x, y and z are the link labels. Purple colored plaquette p consists of sites marked $1-10$. 16

2.5 The diamond lattice: the four links of the lattice are labeled as a (green), b (red), c (black) and d (blue); The sites labeled $\{1, 2, 3, 4, 5, 6, 7, 8, 9, 10\}$ constitute four different plaquettes. 19

3.1 Bipartition scheme in which region A (volume enclosed by the shaded surface) has the topology of a solid sphere. The dashed lines are the links on the boundary. u_{ij} variables on the boundary links are transformed to $w_{A,n}$ and $w_{B,n}$, which are defined on the links (a_{2n-1}, a_{2n}) and (b_{2n-1}, b_{2n}), respectively. 22

3.2 Bipartition scheme in which region A (volume enclosed by the solid surface) is a solid torus. The dashed lines are the links on the boundary. 24

3.3 Various regions considered for the calculation of TEE in the sphere bipartition scheme 25
3.4 Various regions considered for the calculation of TEE in the torus bipartition scheme 25

4.1 Phase diagram in $J_x - J_y$ space with $J_z = 1$. The bulk spectrum is gapless in the shaded regions and gapped elsewhere. 30
4.2 Zigzag edge at the bottom. Periodic boundary condition is imposed in the x- and y- directions. 31
4.3 Bearded edge at the bottom. Periodic boundary condition is imposed in the x- and y- directions. 34
4.4 Armchair edge obtained by cutting the lattice along a plane normal to the x-axis. Periodic boundary condition is imposed in y- and z- directions. . . . 35

List of Tables

4.1 Edge states in different regions of the gapped phase shown in the phase diagram (Fig. 4.1). $[..,..]$ denotes the types of sites at which the wave function is nonvanishing 37

Abbreviations

SSB	Spontaneous Symmetry Breaking
QH	Quantum Hall
QHE	Quantum Hall Effect
TEE	Topological entanglement Entropy
QSL	Quantum Spin Liquid
MZM	Majorana Zero Mode

Nomenclature

S	von Neumann entropy
S_X	von Neumann entropy of the subsystem X
ρ	density matrix of the system
ρ_X	reduced density matrix of the subsystem X
γ	topological entanglement entropy
b_0	zeroth Betti number
b_1	first Betti number
n_X	number of connected components in the subsystem X
ψ	wave function corresponding to sublattice A
ϕ	wave function corresponding to sublattice B
χ	wave function corresponding to sublattice C
τ	wave function corresponding to sublattice D
J_x, J_y, J_z	nearest neighbor coupling constants of the Kitaev model

Chapter 1

Introduction

One of the fundamental tasks of condensed matter physics is the study and classification of different phases of matter. Conventionally the phenomenon of spontaneous symmetry breaking (SSB) introduced by Landau is responsible for characterizing different phases. A local order parameter distinguishes different phases according to their symmetry.

For example, in a liquid to solid transition, liquid has continuous translational symmetry, which is broken down to discrete translational symmetry in the solid. Other examples of SSB include superconductivity, superfluidity, Bose-Einstein condensation, etc.

However, there are exists phases that are not distinguishable based on Landau symmetry breaking theory. An example is the chiral spin states introduced in the context of high temperature superconductivity [1]. They are parity (P) and time-reversal (T) symmetry violating states having the same symmetry and no local order parameter can distinguish different chiral spin states.

Another well-known example of a system having distinct phases but with no local order parameter is in quantum Hall effect. At low temperatures, when a two-dimensional electron gas is subjected to a strong magnetic field the Hall conductance is quantized, taking on values of the form $\nu(e^2/h)$, where the filling factor ν is either an integer or a fraction $\left(\frac{1}{3},\ \frac{2}{5},\ \frac{3}{7},\ \frac{2}{3}, \dots\right)$. Quantum Hall states corresponding to different values of ν all have the same symmetry. The filling factor is related to a topological invariant of the quantum Hall ground state is known as the first Chern number [2, 3].

Phases such as the chiral spin liquid and the quantum Hall states mentioned above, which are characterized by their topological properties and are indistinguishable via a local order parameter, are said to be topologically ordered.

Topologically ordered phases in general have: $1)$ a robust ground state degeneracy that depends on the topology of the underlying space, $2)$ fractional statistics for quasiparticle excitations and $3)$ long-range entanglement.

The celebrated honeycomb lattice spin model of Kitaev [4] is a paradigm system in the study of topological phases. It is an exactly solvable spin-$\frac{1}{2}$ system with excitations that are abelian anyons in one phase and nonabelian anyons in the other phase. In this thesis, we have studied some topological aspects of a three-dimensional generalization of the Kitaev model [5]. In the first part, we have computed the topological entanglement entropy, a quantity that encodes information about the long-range entanglement in the system. In the second part, we have studied gapless excitations localized at the boundary of the system, which are signatures of the nontrivial topology of the bulk, and analyzed their correspondence with the bulk phase.

In the next two sections, we give a brief introduction to topological entanglement entropy and gapless edge states.

1.1 Entanglement Entropy

Quantum entanglement is a phenomenon that occurs in a composite system when the state of some part of the system (a subsystem) cannot be described independently of the rest of the system.

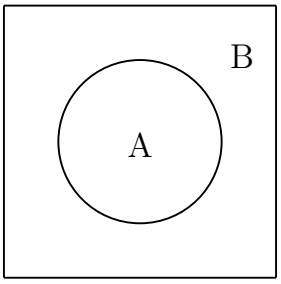

Figure 1.1: Composite system with subsystems A and B

Consider a bipartite system AB composed of subsystems A and B as shown in Figure 1.1. The full Hilbert space $\mathcal{H}$ of the system is the tensor product of the Hilbert spaces $\mathcal{H}_A$ and $\mathcal{H}_B$ of subsystems A and B: $\mathcal{H} = \mathcal{H}_A \otimes \mathcal{H}_B$. Suppose the system is in the pure state $|\psi\rangle$, then we can write $|\psi\rangle$ in terms of basis states $\{|a_A\rangle\}$ and $\{|b_B\rangle\}$, respectively, of $\mathcal{H}_A$ and $\mathcal{H}_B$.

$$|\psi\rangle = \sum_{a,b} \alpha_{a,b} |a_A\rangle |b_B\rangle \tag{1.1}$$

where $\{|a_A\rangle\}$ and $\{|b_B\rangle\}$ with $a = 1, ..., d_A, b = 1, ..., d_B$ form orthonormal bases of $\mathcal{H}_A$

and $\mathcal{H}_B$, respectively. Using Schmidt decomposition method [6], we can write

$$|\psi\rangle = \sum_{i=1}^{d_s} \gamma_i |i_A\rangle |i_B\rangle \tag{1.2}$$

where $\gamma_i,\ i = 1, ..., d_s$, are the Schmidt eigenvalues and they satisfy the conditions $\gamma_i \geq 0$ and $\sum\limits_i \gamma_i^2 = 1$. $d_s \leq \min(d_A, d_B)$ is called the Schmidt rank.

The Schmidt eigenvalues tell us whether subsystems A and B are entangled or not. If only one of the eigenvalues is non zero, then $|\psi\rangle$ is a product (separable) state and A and B are not entangled. On the other hand, if more than one of the eigenvalues are nonzero, then the state is entangled.

The density matrix corresponding to a pure state $|\psi\rangle$ of a composite system is given by

$$\rho = |\psi\rangle\langle\psi|. \tag{1.3}$$

Then the reduced density matrix ρ_A of subsystem A is obtained by tracing out the complimentary system B, i.e.,

$$\rho_A = \text{Tr}_B \rho \tag{1.4}$$

The entanglement entropy (EE) of subsystem A is defined as the von Neumann entropy of ρ_A:

$$S_A = -\text{Tr}(\rho_A \log \rho_A) \tag{1.5}$$

The density matrix of composite system in terms of Schmidt basis is of the form,

$$\rho = \sum_{i,j} \gamma_i \gamma_j |i_A\rangle |i_B\rangle\langle j_A| \langle j_B|$$

and the reduced density matrix of A is

$$\rho_A = \sum_i \gamma_i^2 |i_A\rangle\langle i_A| = \sum_i \lambda_i |i_A\rangle\langle i_A|, \tag{1.6}$$

where $\lambda_i = \gamma_i^2$ is the eigenvalue of ρ_A.

Similarly, we can obtain the reduced density matrix of B by tracing out A:

$$\rho_B = \sum_i \lambda_i |i_B\rangle\langle i_B| \tag{1.7}$$

Since eigenvalues of the reduced density matrix of A and B are same the entanglement entropy of both parts are also the same and we can unambiguously define entanglement entropy S_{AB} between subsystems A and B as

$$S_{AB} = S_A = S_B = -\sum_i \lambda_i \log \lambda_i, \tag{1.8}$$

using Eq. (1.5).

If $|\psi\rangle$ is a product state, then $|\psi\rangle = |i_A\rangle \otimes |i_B\rangle$, and $S_A = S_B = 0$. For entangled states, $S_A \neq 0$. Furthermore, EE is maximum for a maximally entangled state. Thus EE is a measure of the degree of entanglement between the two subsystems.

In general calculating S_A is quite difficult as the trace involves $\log \rho_A$. In some situations we can circumvent this difficulty by using the replica method, which relates S_A to ρ^n via the identity [7]

$$S_A = -\lim_{n\to 1} \frac{\partial}{\partial n} \mathrm{Tr}\rho_A^n \tag{1.9}$$

We will be using the above formula for calculating EE of the Kitaev model.

1.1.1 Topological entanglement entropy

In this thesis, our focus is on EE at zero temperature, i.e., EE of the ground state. When the ground state has an energy gap, the correlation length is finite and the EE S_{AB} between two partitions A and B of the system will get contributions only from a region around the boundary between the two partitions that lie within the correlation length ξ . Consequently, the EE will scale as the "area" of the boundary [8].

In two remarkable papers, Kitaev and Preskill [9] and, independently, Levin and Wen [10] showed that EE in two-dimensional systems has the form

$$S = \alpha L - \gamma, \tag{1.10}$$

where L is the length of the boundary separating the two partitions, and γ is called the

topological entanglement entropy (TEE) and is given by

$$\gamma = \log D, \tag{1.11}$$

where

$$D = \sqrt{\sum_a d_a^2}. \tag{1.12}$$

Here d_a is the quantum dimension of a-type anyon and the summation is over all types of anyonic excitations in the system. The quantity D is called the total quantum dimension. For abelian anyons $d_a = 1$, then D^2 is the total number of anyon types.

For topologically trivial systems, there is only one type of excitation, and which is adiabatically connected to the ground state (vacuum). Then $D = 1$, and $\gamma = 0$. Therefore, a nonzero γ is a signature of topological order.

1.1.2 Extracting topological entanglement entropy

In two dimensions, Topological entanglement entropy γ is the $O(1)$ correction to the term that scales with the length of the boundary in entanglement entropy. γ can be extracted from EE by considering various bipartitions and taking a linear combination of corresponding EE in such a way that the boundary contributions cancel one another and only γ remains. We first describe the scheme used by Kitaev and Preskill [9].

They consider four regions A, B, C and D, whose linear dimensions are large compared to the correlation length (see Figure 1.2). Let S_X denote the von Neumann entropy of subsystem X. Then,

$$S_A + S_B + S_C - S_{AB} - S_{BC} - S_{AC} + S_{ABC} = -\gamma. \tag{1.13}$$

All contributions to the entropy arising from the bulk and the boundaries of various regions mutually cancel and only TEE survives in the linear combination.

Levin and Wen [10] used a different partition scheme by considering four regions $(1-4)$ shown in Figure 1.3. Then, as before,

$$(S_1 - S_2) - (S_3 - S_4) = -\gamma. \tag{1.14}$$

Similar partitioning schemes can be used in three dimensions also for extracting TEE.

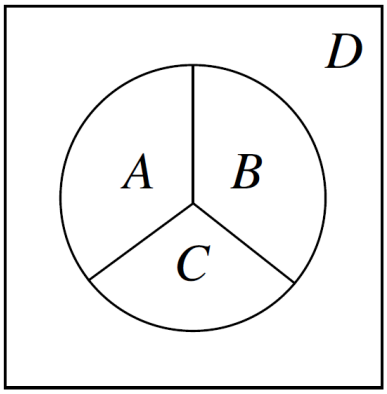

Figure 1.2: The plane is divided into four regions, labeled A, B, C and D (Kitaev and Preskill, 2006).

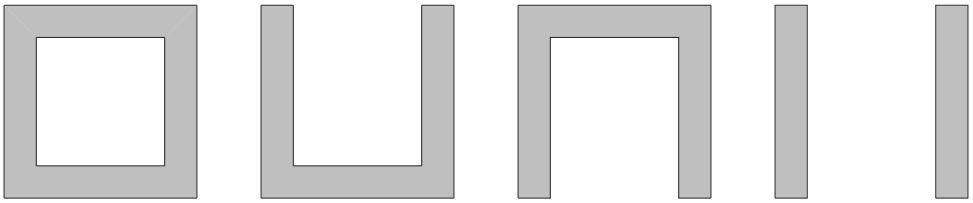

Figure 1.3: Different partitions considered in the Levin-Wen scheme.

This will be discussed in more detail in Chapter 3, when we calculate TEE for 3D Kitaev model.

1.1.3 Topological entanglement entropy in three dimensions

In order to understand the meaning of TEE in three and higher dimensions, Grover et. al. postulated that the total entanglement entropy can be written as sum of a local term and a nonlocal term [11]:

$$S = S_{A,\text{local}} + S_{A,\text{topo}}, \tag{1.15}$$

where $S_{A,\text{local}}$ is the sum over the contributions from the patches located along the boundary of region A.

$$S_{A,\text{local}} = \sum_i S_i. \tag{1.16}$$

They further assumed that S_i, which depends only on the local properties of the boundary, can be expanded in powers of the curvature and its derivatives. Then, using the fact that $S_A = S_{\bar{A}}$ (where $\bar{A}$ is the region complementary to A), they concluded that, in D dimensions, the local contribution to entropy can be written as

$$S_{A,\text{local}} = \alpha_1 L^{D-1} + \alpha_3 L^{D-3} + \alpha_5 L^{D-5} + ... \tag{1.17}$$

The leading term is proportional to the $(D-1)$-dimensional "area" of the boundary. Here only alternate terms in the power series expansion are present. It then immediately follows that in even dimensions there is a constant term in $S_{A,\text{topo}}$ and therefore a constant correction to the area law will correspond to TEE. On the other hand, in three and other odd dimensions, a constant contribution can come from local terms and, therefore, a constant term in EE does not necessarily imply topological order.

1.2 Zero energy Majorana edge modes

The second aspect we study in this thesis is the emergence of gapless edge states in topologically ordered systems. At the interface of two different topological phases, a topological invariant will have different values on either side. Since a topological invariant cannot vary continuously, the only possibility is for the energy gap to close at the boundary. Then, the number of such gapless edge states have a precise correspondence with the bulk topological invaraints [3, 12, 13, 14].

The most well known example of topological edge states is in quantum Hall systems [15, 16, 17, 18]. Other examples include two and three-dimensional topological insulators [19, 20, 21, 22, 23, 24, 25] and a one-dimensional wire with p-wave superconductivity [26].

In this thesis, we have studied gapless edges states in the three-dimensional Kitaev model.

1.3 Outline of the following chapters

In **Chapter 2**, we first review the original Kitaev model on the honeycomb lattice. Then we describe its three-dimensional generalization on the hyperhoneycomb lattice.

In **Chapter 3** we calculate the entanglement entropy of the three-dimensional Kitaev model and then extract the topological entanglement entropy.

In **Chapter 4**, we obtain exact analytical solutions for zero-energy Majorana edge

modes in the three dimensional Kitaev model. We consider different types of edges and establish the correspondence between the bulk and the edge.

In **Chapter 5**, we summarize and discuss the results obtained in the thesis.

Chapter 2

The Kitaev Model

Kitaev's spin-$\frac{1}{2}$ model [4] on the honeycomb lattice is an exactly solvable model that undergoes a quantum phase transition between two topological phases—one supporting abelian anyonic excitations, and the other supporting nonabelian anyons. Kitaev interaction is Ising-like and thus anisotropic, involving only one component of the spin but with the interacting component varying from link to link. What is remarkable about Kitaev model is that nontrivial topological phases can arise from such a simple Hamiltonian involving only two-spin interactions.

There has been various proposals to experimentally realize Kitaev model, viz., in cold atom optical lattices [27, 28], in superconducting circuits [29], and also in some spin rotation invariant systems [30]. In addition, there are several materials such as Na_2IrO_3, Li_2IrO_3, and α-$RuCl_3$ in which Kitaev-type interaction has been observed to be relevant [31, 32, 33, 34, 35, 36, 37, 38, 39, 40].

The Kitaev Hamiltonian has been constructed and solved on some other 2D lattices. These include a triangle-honeycomb lattice [41], a mosaic structure lattice [42], and a two layer stacked honeycomb lattice [43].

Kitaev model has also been generalized to three dimensions. In this thesis we have studied topological properties of the Kitaev model on the hyperhoneycomb lattice [5], a three-dimensional lattice that shares some features of the honeycomb lattice (such as coordination number 3) that are essential for the construction of the Kitaev Hamiltonian. The Kitaev Hamiltonian on the hyperhoneycomb lattice with additional Heisenberg interactions has been proposed as a model for the iridium oxide β-Li_2IrO_3 [44, 45, 46]. There are other three-dimensional generalizations of the Kitaev model [47, 48, 49]

In the following sections of this chapter we review the construction and solution of the Kitaev Hamiltonian in both two and three dimensions.

2.1 Kitaev Hamiltonian

The Kitaev model consists of spin-$1/2$ variables located at the sites of a honeycomb lattice [4]. These spin-$1/2$ degree of freedom can be represented by Pauli matrices σ^x, σ^y, and σ^z at each lattice site. Because of trigonal connectivity of honeycomb lattice, there are three types of links distinguished by their orientations, which are labeled $x,\ y$ and z as shown in Figure. 2.1. The Hamiltonian is defined to be

$$H = -J_x \sum_{x-\text{link}} \sigma_i^x \sigma_j^x - J_y \sum_{y-\text{link}} \sigma_i^y \sigma_j^y - J_z \sum_{z-\text{link}} \sigma_i^z \sigma_j^z \tag{2.1}$$

where J_x, J_y and J_z are positive nearest neighbor coupling constants.

The elementary loop, called a plaquette, in the honeycomb lattice is hexagon. For each plaquette p we define a plaquette operator W_p as

$$W_p = \sigma_1^x \sigma_2^y \sigma_3^z \sigma_4^x \sigma_5^y \sigma_6^z, \tag{2.2}$$

where the sites are labeled as in the plaquette shown in Figure 2.1. In W_p, at each site on the plaquette the spin component of the Pauli matrix is same as the label of the outgoing link at that site. It is straightforward to show that the plaquette operators commute with each other as well as with Hamiltonian, that is, $[W_p, W_{p'}] = 0,\ [W_p, H] = 0,\ \ \forall p, p'$. Therefore, the Hamiltonian becomes block-diagonal in the eigenbasis of the plaquette operators. Since $W_p^2 = 1$, its eigenvalues, denoted w_p, are ± 1.

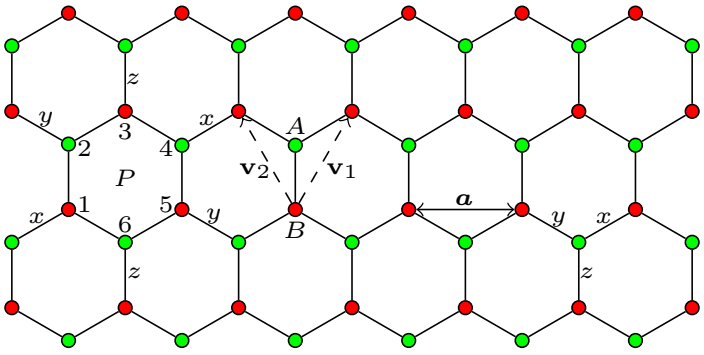

Figure 2.1: Honeycomb lattice: the two sites labeled A(green) and B(red) belong to a unit cell; $\mathbf{v}_1$, and $\mathbf{v}_2$ are basis vectors; x, y and z are the link labels. Plaquette p consists of sites marked $1-6$.

2.1.1 Hamiltonian in Majorana fermion representation

To diagonalize the Hamiltonian, we use a Majorana fermion representation of the the spin-$\frac{1}{2}$ operators. At each site j we introduce four Majorana fermion operators $\gamma_j^x, \gamma_j^y, \gamma_j^z$, and η_j. The Majorana operators obey the following algebra: $\{\gamma_i^\alpha, \gamma_j^\beta\} = 2\delta_{ij}\delta_{\alpha\beta}$, $\{\gamma_i^\alpha, \eta_j\} = 0$, $(\gamma_i^\alpha)^2 = 1$ and $\eta_i^2 = 1$. The Hilbert space corresponding to four Majorana fermions is four-dimensional whereas the spin Hilbert space has dimension 2. In the enlarged fermion Hilbert space, we define spin operators as

$$\widetilde{\sigma}_j^\alpha = i\gamma_j^\alpha \eta_j. \tag{2.3}$$

The operator $D_j = \gamma_j^x \gamma_j^y \gamma_j^z \eta_j$ commutes with $\widetilde{\sigma}_j^\alpha$ and in the subspace corresponding to $D_j = 1$, it can be easily shown that $\widetilde{\sigma}_j^\alpha$ obey the algebra of Pauli matrices. Thus, we can write the Hamiltonian in terms of $\widetilde{\sigma}_j^\alpha$ operators in the enlarged Hilbert space, and the physical space then corresponds to $D_j = 1$.

In the Majorana representation the Hamiltonian becomes

$$\widetilde{H} = \frac{i}{2} \sum_{jk} J_{\alpha_{jk}} \hat{u}_{jk} \eta_j \eta_k, \tag{2.4}$$

where α_{jk} is the label of the $j-k$ link, and $\hat{u}_{jk} = i\gamma_j^{\alpha_{jk}} \gamma_k^{\alpha_{jk}}$.

The link operators $\hat{u}_{jk}$ are Hermitian and antisymmetric in the i, j indices:

$$\hat{u}_{jk} = -\hat{u}_{kj}, \;\; \hat{u}_{jk}^2 = 1, \;\; \hat{u}_{jk}^\dagger = \hat{u}_{jk}. \tag{2.5}$$

Moreover, $[\hat{u}_{jk}, \hat{u}_{lm}] = 0$ and $[\hat{u}_{jk}, \widetilde{H}] = 0$. Then, in the eigenbasis of $\hat{u}_{jk}$, in a particular sector having eigenvalues u_{jk}, the Hamiltonian becomes

$$\widetilde{H}(\{u_{jk}\}) = \frac{i}{2} \sum_{jk} J_{\alpha jk} u_{jk} \eta_j \eta_k \tag{2.6}$$

We have mapped the spin model to a system of free fermions in the presence of a static Z_2 gauge field.

2.1.2 Ground state

To find the ground state, we first note that the Hamiltonian $\widetilde{H}$ has a Z_2 gauge symmetry, where the operator D_j is the gauge transformation at j. The elements of the gauge group

can be written as $\prod_j D_j^{n_j}$, with $n_j = 0$ or 1. Then the physical states $|\psi_{phys}\rangle$ are the gauge invariant states, i.e., $D_j|\psi_{phys}\rangle = |\psi_{phys}\rangle$.

Under a gauge transformation, $u_{ij} \rightarrow X_i u_{ij} X_j$, where $X_i = (1 - 2n_i)$. The gauge invariant quantities then are the Wilson-loop variables $W_l = \Pi_{<ij>} u_{ij}$, where $< ij >$ are the links belonging to the loop l. Based on a theorem by Lieb [50], it has been shown that the ground state corresponds to $W_p = 1$ for all plaquettes p [4]. To get the physical ground state, we first find the lowest energy state in any one of the $\{u_{ij}\}$ configuration for which $W_p = 1$ for all p, and then project it to $D_j = 1$ subspace.

The total Hilbert space is the tensor product of the gauge sector and the fermion sector. Let u denote a $\{u_{ij}\}$ configuration for which $W_p = 1$ and $\phi(u)$ be the corresponding lowest energy fermion wave function. Then the normalized ground state is (assuming periodic boundary conditions)

$$|\psi\rangle = \frac{1}{\sqrt{2^{N+1}}} \prod_j \left(\frac{1 + D_j}{2}\right) |u\rangle \otimes |\phi(u)\rangle = \frac{1}{\sqrt{2^{N+1}}} \sum_g D_g |u\rangle \otimes |\phi(u)\rangle, \tag{2.7}$$

where g denotes a subset of the lattice sites, the summation is over all possible such subsets, and

$$D_g = \prod_{j \in g} D_j. \tag{2.8}$$

2.1.3 Energy spectrum and phase diagram

Since $W_p = 1$ in the ground state, we can choose $u_{jk} = 1$ for all links. In this sector the Hamiltonian becomes

$$H = \frac{i}{2} \sum_{jk} J_{\alpha jk} \eta_j \eta_k. \tag{2.9}$$

In order to calculate the excitation spectrum we have to first explicitly express the lattice sites in terms of a set of basis vectors. We choose the two sites on an z-link to be a unit cell and

$$\mathbf{v}_1 = \frac{a}{2}\hat{i} + \frac{\sqrt{3}a}{2}\hat{j}, \text{ and}$$
$$\mathbf{v}_2 = -\frac{a}{2}\hat{i} + \frac{\sqrt{3}a}{2}\hat{j}$$

to be the basis vectors of the underlying triangular Bravais lattice (see Figure 2.1). Denoting the lattice vector of a unit cell by $\mathbf{r}$, the two sites within the unit cell are located at $\mathbf{r} + \frac{a}{\sqrt{3}}\hat{j}$ (A-sublattice) and $\mathbf{r}$ (B-sublattice). Further, we relabel the η_j Majorana operators as a_j when $j \in A$, and as b_j when $j \in B$. Then the Hamiltonian in Eq. (2.9) becomes

$$H = i \sum_{\mathbf{r}} \Big[J_x a_{\mathbf{r}} b_{\mathbf{r}+\mathbf{v}_1} + J_y a_{\mathbf{r}} b_{\mathbf{r}+\mathbf{v}_2} + J_z a_{\mathbf{r}} b_{\mathbf{r}} \Big] \tag{2.10}$$

After making the following Fourier transform,

$$\begin{aligned} a_{\mathbf{r}} &= \sum_{\mathbf{k} \in \frac{1}{2}BZ} (a_{\mathbf{k}} e^{i\mathbf{k}.(\mathbf{r}+\frac{a}{\sqrt{3}}\hat{j})} + a^{\dagger}_{\mathbf{k}} e^{-i\mathbf{k}.(\mathbf{r}+\frac{a}{\sqrt{3}}\hat{j})}), \\ b_{\mathbf{r}} &= \sum_{\mathbf{k} \in \frac{1}{2}BZ} (b_{\mathbf{k}} e^{i\mathbf{k}.\mathbf{r}} + b^{\dagger}_{\mathbf{k}} e^{-i\mathbf{k}.\mathbf{r}}), \end{aligned}$$

(where the $\mathbf{k}$-summation is only over half of the Brillouin zone (BZ) since $a^{\dagger}_{\mathbf{k}} = a_{-\mathbf{k}}$) the Hamiltonian is brought to the form $H = \sum_{\mathbf{k}} \phi^{\dagger}_{\mathbf{k}} H_{\mathbf{k}} \phi_{\mathbf{k}}$, where $\phi^{\dagger}_{\mathbf{k}} = \begin{bmatrix} a^{\dagger}_{\mathbf{k}} & b^{\dagger}_{\mathbf{k}} \end{bmatrix}$ and

$$H_{\mathbf{k}} = \begin{bmatrix} 0 & if(\mathbf{k}) \\ -if^*(\mathbf{k}) & 0 \end{bmatrix}, \tag{2.11}$$

with

$$f(\mathbf{k}) = 2 \left(J_x e^{i\left(\frac{k_x a}{2} + \frac{k_y a}{2\sqrt{3}}\right)} + J_y e^{-i\left(\frac{k_x a}{2} - \frac{k_y a}{2\sqrt{3}}\right)} + J_z e^{-i\frac{k_y a}{\sqrt{3}}} \right). \tag{2.12}$$

Then the energy dispersions are

$$\begin{aligned} E_{\mathbf{k}} = \pm|f(\mathbf{k})| = \pm 2 \Bigg[J_x^2 + J_y^2 + J_z^2 + 2J_x J_y \cos(k_x a) + 2J_y J_z \cos\left(\frac{k_x a}{2} - \frac{\sqrt{3}}{2} k_y a\right) \\ + 2J_x J_z \cos\left(\frac{k_x a}{2} + \frac{\sqrt{3}}{2} k_y a\right) \Bigg]^{1/2}. \end{aligned} \tag{2.13}$$

In the ground state, the negative energy band is completely filled. Then, for the excitation spectrum to be gapless, $f(\mathbf{k}) = 0$ for some value of $\mathbf{k}$. This equation has a solution if

and only if $|J_x|,\ |J_y|$ and $|J_z|$ satisfy the triangular inequalities:

$$|J_z| \leq |J_x| + |J_y|, |J_x| \leq |J_y| + |J_z|, |J_y| \leq |J_x| + |J_z| \tag{2.14}$$

Figure.(2.2) depicts the phase diagram on the plane $J_x + J_y + J_z = 1$.

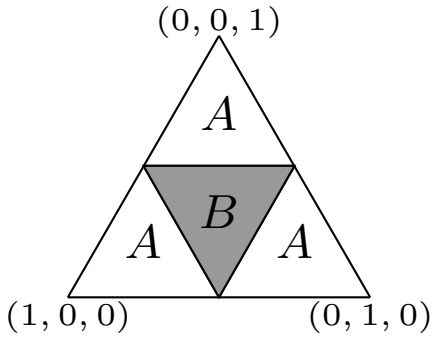

Figure 2.2: Phase diagram on the plane $J_x + J_y + J_z = 1$. Region A is gapped and region B gapless.

2.1.4 Excitations in the gapped phase

The nature of excitations in the gapped phase can be understood by considering the limit of one of the couplings being very large compared to the other two, e.g., $J_z >> J_x, J_y$.

When $J_x = J_y = 0$, the system consists of decouple $z-link$ dimers and the each dimer has two degenerate ground states: $|\uparrow\uparrow\rangle$ and $|\downarrow\downarrow\rangle$, where

$$\sigma^z|\uparrow\rangle = |\uparrow\rangle, \quad \sigma^z|\downarrow\rangle = -|\downarrow\rangle \tag{2.15}$$

In the limit $J_z >> J_x, J_y$ the low energy states of the will be described by an effective Hamiltonian acting in the above degenerate space, the basis states of which can be labeled by the eigenvalues of a pseudospin variable τ^z defined as follows:

$$\tau^z|\uparrow\uparrow\rangle = |\uparrow\uparrow\rangle \tag{2.16}$$

$$\tau^z|\downarrow\downarrow\rangle = -|\downarrow\downarrow\rangle. \tag{2.17}$$

To leading order in perturbation theory, the effective Hamiltonian is [4]

$$H_{\text{eff}} = -\frac{J_x^2 J_y^2}{16|J_z|^3} \sum_p Q_p, \quad Q_p = \tau_i^y \tau_j^y \tau_k^z \tau_l^z \tag{2.18}$$

The pseudospins reside on the links of a square lattice and H_{eff} given above is (after a unitary transformation) exactly the toric code [51]:

$$H_{toric} = -J' \left(\sum_s A_s + \sum_p B_p \right), \tag{2.19}$$

where $A_s = \prod_{j \in s} \tau_j^x$ is the product of the four τ^x operators at the vertex s and $B_p = \prod_{j \in p} \tau_j^z$ is the product of the four τ^z operators on the plaquette p (see Figure.(2.3). All A_s and B_p

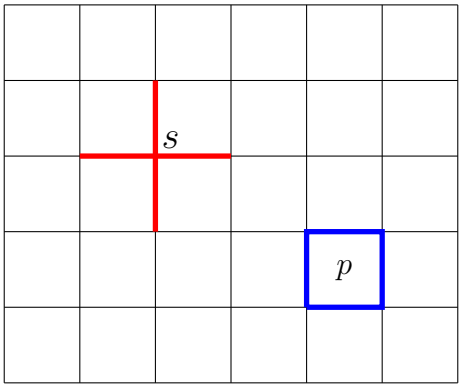

Figure 2.3: Square lattice on the torus; s represents the star operator; p represents the plaquette operator.

operators commute with each other and satisfy the constraints

$$\prod_s A_s = 1, \quad \prod_p B_p = 1. \tag{2.20}$$

In the ground state $A_s = 1$ and $B_p = 1$. The excitations are the e-particles (A_s excitations) and the m-particles (B_p excitations). e and m particles behave as bosons when exchanged among the same type, but e and m particles mutually obey anyon statistics: an e-particle on braiding around an m-particle generates a phase of π. Further, the fusion of an e-particle and an m-particle ($\epsilon = e \times m$) is a fermion.

The toric code therefore has four superselection sectors: 1 (vacuum), e, m, and ϵ.

2.2 Three dimensional Kitaev Model

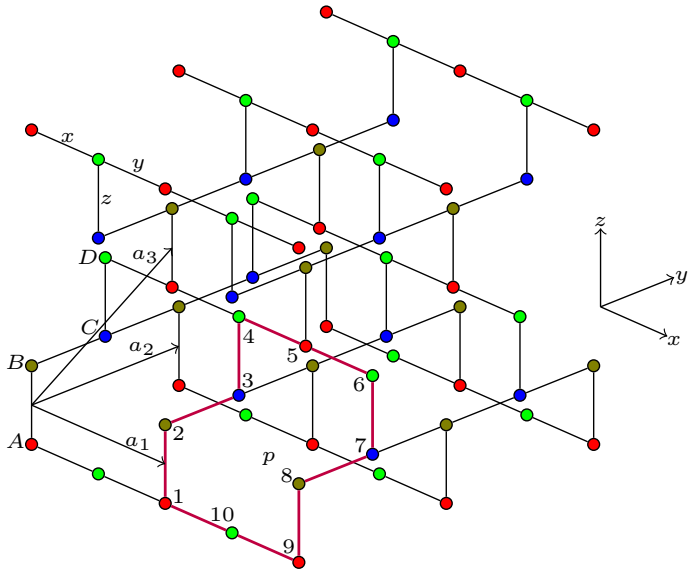

Figure 2.4: The 3D lattice: the four sites labeled A(red), B(yellow), C(blue) and D(green) belong to a unit cell; a_1, a_2, a_3 are the basis vectors; x, y and z are the link labels. Purple colored plaquette p consists of sites marked $1-10$.

In general, Kitaev Hamiltonian can be defined on any trivalent lattice, independent of the dimension. In three dimensions, one of the simplest such lattice is the hyperhoneycomb lattice (see Figure 2.4. Note that the lattice depicted here have straight chains lying in the x-y plane, whereas in the actual hyperhoneycomb lattice they have a zig-zag structure. However, the connectivity of the two lattices are the same). Kitaev model defined on this lattice is also exactly solvable [5], owing to the existence of an infinite number of conserved plaquette operators, analogous to those in the honeycomb lattice.

We can label the links as x, y or z in such a way that the three links at each site will have different labels (see Figure 2.4). Then, formally the Hamiltonian is defined in the same way as in 2D:

$$H = -J_x \sum_{x-\text{link}} \sigma_j^x \sigma_k^x - J_y \sum_{y-\text{link}} \sigma_j^y \sigma_k^y - J_z \sum_{z-\text{link}} \sigma_j^z \sigma_k^z \tag{2.21}$$

The elementary loop (plaquette) in the hyperhoneycomb lattice has 10 sites, as shown in (see Figure 2.4), and we define a plaquette operator W_p similar to 2D as follows.

$$W_p = \sigma_1^x \sigma_2^y \sigma_3^y \sigma_4^y \sigma_5^z \sigma_6^x \sigma_7^y \sigma_8^y \sigma_9^y \sigma_{10}^z. \tag{2.22}$$

As before, W_p operators commute with each other as well as with the Hamiltonian.

Writing the Hamiltonian in the Majorana fermion representation, in a particular eigenvalue sector of the link operators $\hat{u}_{ij}$ we get a quadratic Hamiltonian in terms of the η_j operators. The ground state is again found to be in the uniform flux sector, as before [5].

An unit cell of the hyperhoneycomb lattice contains 4 lattice sites. We label them $A,\ B,\ C,\ D$ and the corresponding η_j operators as $a_j,\ b_j,\ c_j,\ d_j$, respectively. Then, in $u_{ij} = 1$ sector, the Hamiltonian becomes

$$H = i \sum_{\mathbf{r}} \Big[J_x (a_{\mathbf{r}} d_{\mathbf{r}-\mathbf{a}_3} + c_{\mathbf{r}} b_{\mathbf{r}}) + J_y (a_{\mathbf{r}} d_{\mathbf{r}+\mathbf{a}_1-\mathbf{a}_3} + c_{\mathbf{r}} b_{\mathbf{r}+\mathbf{a}_2}) + J_z (a_{\mathbf{r}} b_{\mathbf{r}} + c_{\mathbf{r}} d_{\mathbf{r}})]. \tag{2.23}$$

Using the following Fourier transform,

$$\begin{aligned}
a_{\mathbf{r}} &= \sum_{\mathbf{k} \in \frac{1}{2}BZ} (a_{\mathbf{k}} e^{i\mathbf{k}.\mathbf{r}} + a^\dagger_{\mathbf{k}} e^{-i\mathbf{k}.\mathbf{r}}), \\
b_{\mathbf{r}} &= \sum_{\mathbf{k} \in \frac{1}{2}BZ} (b_{\mathbf{k}} e^{i\mathbf{k}.(\mathbf{r}+\hat{\mathbf{z}})} + b^\dagger_{\mathbf{k}} e^{-i\mathbf{k}.(\mathbf{r}+\hat{\mathbf{z}})}), \\
c_{\mathbf{r}} &= \sum_{\mathbf{k} \in \frac{1}{2}BZ} (c_{\mathbf{k}} e^{i\mathbf{k}.(\mathbf{r}+\hat{\mathbf{y}}+\hat{\mathbf{z}})} + c^\dagger_{\mathbf{k}} e^{-i\mathbf{k}.(\mathbf{r}+\hat{\mathbf{y}}+\hat{\mathbf{z}})}), \\
d_{\mathbf{r}} &= \sum_{\mathbf{k} \in \frac{1}{2}BZ} (d_{\mathbf{k}} e^{i\mathbf{k}.(\mathbf{r}+\hat{\mathbf{y}}+2\hat{\mathbf{z}})} + d^\dagger_{\mathbf{k}} e^{-i\mathbf{k}.(\mathbf{r}+\hat{\mathbf{y}}+2\hat{\mathbf{z}})}),
\end{aligned}$$

the Hamiltonian becomes of the form $H = \sum_{\mathbf{k} \in \frac{1}{2}BZ} \phi^\dagger_{\mathbf{k}} H_{\mathbf{k}} \phi_{\mathbf{k}}$, where $\phi^\dagger_{\mathbf{k}} = \begin{bmatrix} a^\dagger_{\mathbf{k}} & c^\dagger_{\mathbf{k}} & b^\dagger_{\mathbf{k}} & d^\dagger_{\mathbf{k}} \end{bmatrix}$ and

$$H_{\mathbf{k}} = 2i \begin{bmatrix}
0 & 0 & J_z e^{ik_z} & J_x e^{-ik_x} + J_y e^{ik_x} \\
0 & 0 & J_x e^{-ik_y} + J_y e^{ik_y} & J_z e^{ik_z} \\
-J_z e^{-ik_z} & -J_x e^{ik_y} - J_y e^{-ik_y} & 0 & 0 \\
-J_x e^{ik_x} - J_y e^{-ik_x} & -J_z e^{-ik_z} & 0 & 0
\end{bmatrix}. \tag{2.24}$$

Solving for the spectrum, we get

$$E_{\mathbf{k}}^2 = \pm 2\Bigg[\Big\{J_x^2+J_y^2+J_z^2+2J_xJ_y\cos(k_x+k_y)\cos(k_y-k_x)\Big\} \pm 4\Big\{J_x^2J_y^2+2J_x^2J_z^2+2J_y^2J_z^2 \\ + 2J_xJ_yJ_z^2\Big[2\cos(k_x+k_y)\cos(k_y-k_x)+\cos(k_x-k_y+2k_z)+\cos(k_x-k_y-2k_z)\Big] \\ + J_x^2J_y^2\Big[\cos 2(k_x+k_y)\cos 2(k_x-k_y)-\cos 2(k_x+k_y)-\cos 2(k_x-k_y)\Big] \\ + 2J_x^2J_z^2\cos(k_x+k_y+2k_z)+2J_y^2J_z^2\cos(k_x+k_y-2k_z)\Big\}^{1/2}\Bigg]^{1/2}. \tag{2.25}$$

In the ground state, the two negative energy bands are completely filled and the condition for the spectrum to be gapless is

$$J_z^2\, e^{i2k_z} - (J_x e^{-ik_x} + J_y e^{ik_x})(J_x e^{-ik_y} + J_y e^{ik_y}) = 0. \tag{2.26}$$

The above condition can be satisfied for some $\mathbf{k}$ only when

$$|J_x| \le |J_y| + |J_z|, \;\; |J_y| \le |J_z| + |J_x|, \;\; |J_z| \le |J_x| + |J_y|. \tag{2.27}$$

Thus we get the same phase diagram as in 2D (Figure 2.2). When Inequality (4.10) is satisfied, $E(\mathbf{k})$ vanishes along a loop in $\mathbf{k}$-space determined by Eq. (4.9), and the dispersion is linear in $|\mathbf{k}|$ away from the gapless loop [5].

2.2.1 Excitations in the gapped phase

As in the two dimensional case, the excitations in the gapped phase can be studied using perturbation theory in the limit $J_z \ll J_x, J_y$. We then obtain an effective Hamiltonian in terms of the pseudospin operators τ^α defined in Eq. (2.17). (The pseudospin variables reside on the z-links.) The effective Hamiltonian is [52]

$$H_{\text{eff}} = -\frac{7J_x^4J_y^2}{256J_z^5}\sum_p B_p - \frac{7J_y^4J_x^2}{256J_z^5}\sum_p{}' B_p \tag{2.28}$$

where the unprimed sum is over plaquettes containing four x-links and two y-links, while the primed sum is over plaquettes containing two x-links and four y-links involved. This Hamiltonian can be mapped to a $3D$ toric code defined on a diamond lattice [52] (see Fig-

ure. 2.5). Due to certain nontrivial constraints on the plaquette operators B_p, the excited

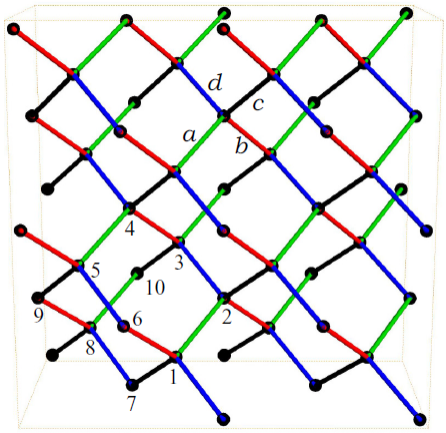

Figure 2.5: The diamond lattice: the four links of the lattice are labeled as a (green), b (red), c (black) and d (blue); The sites labeled $\{1, 2, 3, 4, 5, 6, 7, 8, 9, 10\}$ constitute four different plaquettes.

plaquettes form closed loops (in a dual lattice in which the links correspond to plaquettes in the original lattice). Moreover, the elementary plaquette-loop, consisting of six excited plaquettes, cannot be created by a local operation on the ground state, and they obey fermionic statistics.

Chapter 3

Topological Entanglement Entropy

In two dimensions, the leading term in entanglement entropy is proportional to the length of the boundary and the $O(1)$ correction to it is the topological entanglement entropy (TEE), as we have discussed in Sec.1.1.1. A natural question then is: In higher dimensions D, in particular for $D = 3$, does a constant term in entanglement entropy imply topological order? Grover et al [11] have addressed this question and, based on an expansion of local contributions to the entropy in terms of curvature and its derivatives, they have found that in three dimensions (or in any odd dimensions) a constant can arise in a generic gapped system purely from local correlations. That is, a nonzero γ does not necessarily imply topological order.

The boundary of a three-dimensional (3D) system is two dimensional and 2D manifolds are characterized by two topological invariants: zeroth Betti number b_0 (number of connected components) and the first Betti number b_1 (number of noncontractible loops). The TEE, in general, can depend on both the invariants:

$$S = \alpha A - b_0\gamma_0 + \frac{b_1}{2}\gamma_1 \tag{3.1}$$

where A is the area of the boundary, and α, γ_0 and γ_1 are constants. However, for compact surfaces b_0 and b_1 are not independent and are related through the Euler characteristic, $\chi = 2b_0 - b_1$, which can be thought of as a sum of local terms and therefore be absorbed into the area term; thus γ_0 and γ_1 are not independent topological entropies [11].

Even though trivial phases in 3D may also give rise to a constant term in the entropy, the topological contribution can still be extracted by considering various carefully chosen partitioning of the system and then taking an appropriate linear combination of the corresponding entropies [9, 10, 53, 11]. In the process local, non-topological contributions are eliminated.

In three dimensions, TEE has been calculated for some exactly solvable models. These include: the cubic lattice toric code[53], general quantum double models[54, 55, 11], and Walker-Wang models[56, 57, 58]. In all these cases, $\gamma_0 = \ln \mathcal{D}$, which is similar to the general case in two dimensions ($\mathcal{D}$ being the total quantum dimension). TEE has also been calculated[59] for three-dimensional Ryu-Kitaev model[47], which is a generalization of Kitaev's honeycomb lattice model[4]. However, for this model it is not clear to us what the total quantum dimension is and we have not been able to check the above relation. It is then interesting to examine other three-dimensional models and see whether such a relation between TEE and $\mathcal{D}$ exists or not.

In this chapter we present our results on TEE of three-dimensional Kitaev model on the hyperhoneycomb lattice.

3.1 Entanglement entropy

We start with the ground state of the 3D Kitaev model (see Sec. 2.1.2).

$$|GS\rangle = \frac{1}{\sqrt{2^{N+1}}} \sum_g D_g |u\rangle \otimes \phi(u)\rangle, \tag{3.2}$$

We now calculate entanglement entropy for the above ground state. Our calculation is a straightforward generalization of Yao and Qi's computation for the two-dimensional Kitaev model[60], from hereon referred to as YQ.

Entanglement entropy S between two partitions A and B of a system is defined as the von Neumann entropy of the reduced density matrix of one of the partitions:

$$S = -\mathrm{Tr}\ \rho_A \ln \rho_A, \tag{3.3}$$

where $\rho_A = \mathrm{Tr}_B\ \rho$, with Tr_B denoting partial trace with respect to partition B, and $\rho = |GS\rangle\langle GS|$ is the total density matrix. Note that S is symmetric under the interchange of A and B, i.e., we can also write $S = -\mathrm{Tr}\ \rho_B \ln \rho_B$, where $\rho_B = \mathrm{Tr}_A\ \rho$.

We now briefly go through the steps in YQ and show that their calculation can be readily extended to the hyperhoneycomb lattice.

They calculated entanglement entropy using the following replica method formula[8]:

$$S = -\mathrm{Tr}_A[\rho_A \log \rho_A] = -\frac{\partial}{\partial n} \mathrm{Tr}_A[\rho_A^n]\Big|_{n=1} \tag{3.4}$$

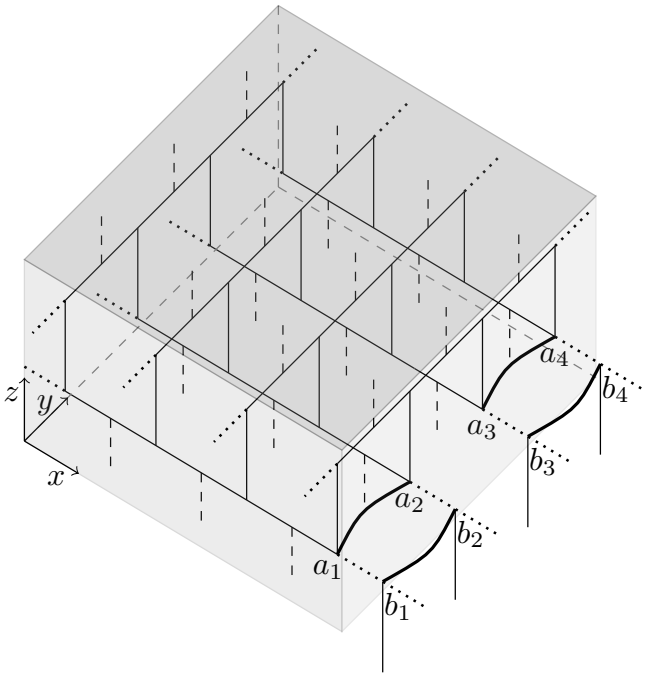

Figure 3.1: Bipartition scheme in which region A (volume enclosed by the shaded surface) has the topology of a solid sphere. The dashed lines are the links on the boundary. u_{ij} variables on the boundary links are transformed to $w_{A,n}$ and $w_{B,n}$, which are defined on the links (a_{2n-1}, a_{2n}) and (b_{2n-1}, b_{2n}), respectively.

To obtain ρ_A we need to do the partial trace over B, Tr_B, and for that we require a set of basis vectors of the form $|\psi^i\rangle_A \otimes |\chi^i\rangle_B$. But the gauge field u_{ij} are located at the links and in any partitioning of the lattice into two regions A and B, there will be some links straddling both A and B. To get around this, YQ transformed each pair of u_{ij} on the shared links into two new variables, one of them defined on a link lying entirely in region A and the other in B. This is a crucial step in their calculation and is not specific to two dimensions. In the 3D lattice also the links shared by both regions can be similarly paired and the corresponding gauge variables can then be transformed to links lying entirely in either A or B (see Fig. 3.1). This procedure will be made more precise when we calculate S_G, the contribution to entanglement entropy from the gauge sector, in the appendix A.

The calculation for the hyperhoneycomb lattice proceeds exactly as in YQ and we can directly take their following main result (for details we refer to their paper[60] and the associated supplementary material):

$$\mathrm{Tr}_A[\rho_A^n] = \mathrm{Tr}_{A,G}[\rho_{A,G}^n] \cdot \mathrm{Tr}_{A,F}[\rho_{A,F}^n], \tag{3.5}$$

where $\rho_{A,F} = \mathrm{Tr}_B|\phi(u)\rangle\langle\phi(u)|$ and $\rho_{A,G} = \mathrm{Tr}_B|G(u)\rangle\langle G(u)|$ are, respectively, the reduced density matrix for the Majorana fermion wave function $|\phi(u)\rangle$ and for the state $|G(u)\rangle = \left(1/\sqrt{2^{(N-1)}}\right)\sum_{\tilde{u}}|\tilde{u}\rangle$ in the gauge sector. Here $\tilde{u}$ summation is over all gauge field configurations gauge equivalent to u.

From Eqs. (3.4) and (3.5) it immediately follows that the entanglement entropy $S = S_G + S_F$, where S_G is the entanglement entropy of the gauge part and S_F that of the fermionic part. YQ have further shown that S_F has no constant term independent of the length/area of the boundary, therefore, S_F does not contribute to TEE.

Calculation of S_G proceeds in exactly the same way as in YQ and the details are given in the appendix A. In our calculation, we also obtain the dependence of TEE on b_0 and b_1. Finally, we get

$$S_G = L\ln 2 - b_0 \ln 2, \tag{3.6}$$

where $2L$ is the number of links on the boundary. Thus S_G depends only on b_0 but not on b_1.

3.2 Topological entanglement entropy

As discussed in the introduction, the constant term by itself is not a signature of topological order[11]. Moreover, in the expression for S in general it is difficult to unambiguously separate the area term and the constant. However, TEE can still be extracted using a scheme introduced for 2D systems in Refs. [9] and [10]. Here we follow a generalization of this scheme to three dimensions[53].

The basic idea is to consider a few different regions of the lattice and then to take a linear combination of corresponding entanglement entropies in such a way that all the surface contributions mutually cancel and the resultant entity is a topological invariant, which can then be taken as the topological entanglement entropy of the system.

We consider two different bipartitions in which region A is: 1) a spherical shell, which is nontrivial with respect to closed surfaces, and 2) a solid torus, which is nontrivial with respect to closed loops (see Fig. 3.2). In the first case we consider the four regions in A shown in Fig. 3.3 (1-4). Let S_i be the entanglement entropy corresponding to the i^{th} region. Then using Eq. (3.6) we obtain TEE, $S^{(1)}_{top}$, as

$$S^{(1)}_{top} = -S_1 + S_2 + S_3 - S_4 = \ln 2. \tag{3.7}$$

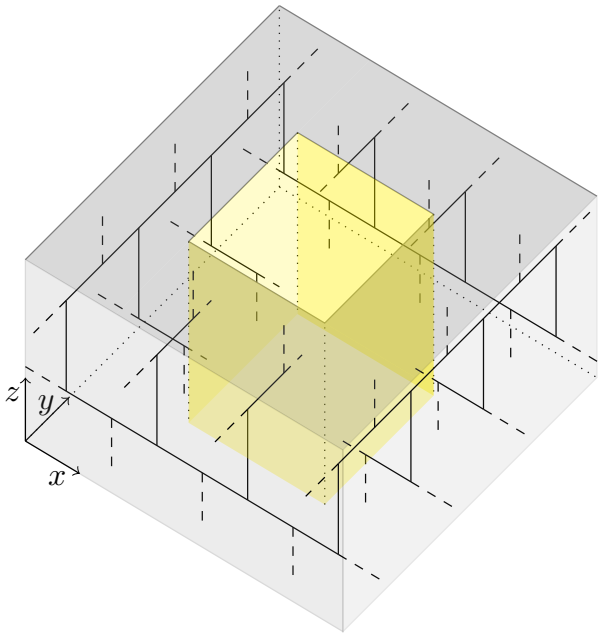

Figure 3.2: Bipartition scheme in which region A (volume enclosed by the solid surface) is a solid torus. The dashed lines are the links on the boundary.

In the second case we consider the regions (5-8) shown in Fig. 3.4, and we get

$$S_{top}^{(2)} = -S_5 + S_6 + S_7 - S_8 = \ln 2. \tag{3.8}$$

In both the schemes the boundary contributions from various regions cancel in S_{top} and it is thus invariant under continuous deformations[9, 10].

Thus we have obtained γ_0 [defined in Eq. (3.1)] to be $\ln 2$. However, γ_0 is not equal to $\ln \mathcal{D}$, where the total quantum dimension $\mathcal{D}$ for our model is $\sqrt{2}$.

The total quantum dimension of 3D Kitaev model is obtained as follows: In the limit $J_z \gg J_x, J_y$, Kitaev model maps to a toric-code-type Hamiltonian on the diamond lattice[5]. This Hamiltonian is a sum of mutually commuting plaquette operators, denoted B_p, the eigenvalues of which are ± 1. In the ground state $B_p = +1$ for all plaquettes.

Certain local constraints demand that those plaquettes for which $B_p = -1$ must form a closed loop in a dual lattice, in which the links represent plaquettes in the original lattice. Thus the excitations form "flux" tubes. Furthermore, a global constraint prohibits creation of a single elementary flux tube, consisiting of six excited plaquettes; they can only be created in pairs. Therefore, an elementary flux tube is in a superselection sector different from vacuum. There are no other type of elementary excitations and the total number of superselection sectors is two. Consequently, the total quantum dimension of the model is

$\sqrt{2}$.

Here we note that, since $\gamma_0 = \ln 2$ is independent of J_x, J_y and J_z, γ_0 has the same value for the diamond lattice toric code also.

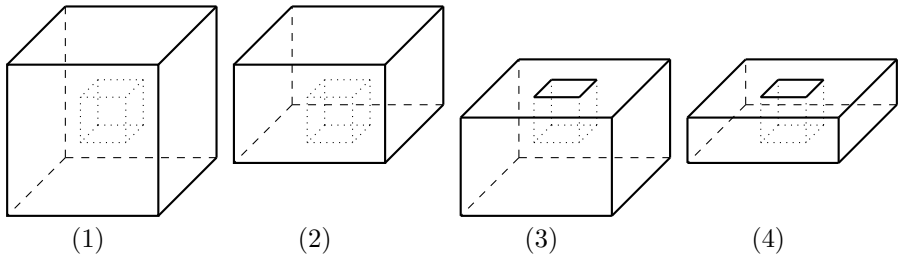

Figure 3.3: Various regions considered for the calculation of TEE in the sphere bipartition scheme

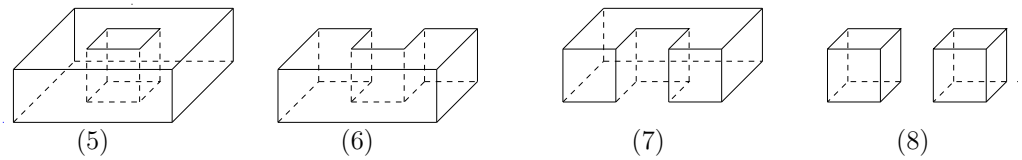

Figure 3.4: Various regions considered for the calculation of TEE in the torus bipartition scheme

3.3 Summary

We have calculated the topological entanglement entropy for a three-dimensional hyper-honeycomb lattice generalization of Kitaev's honeycomb lattice model. We have found that γ_0, the part of TEE proportional to b_0, is $\ln 2$. The total quantum dimension $\mathcal{D}$ of this model is $\sqrt{2}$ and therefore it provides an example of a 3D system in which the relation $\gamma_0 = \ln \mathcal{D}$ does not hold.

Since $\gamma_0 = \ln 2$, it is tempting to interpret it as $\ln |Z_2|$, which is the TEE for a class of discrete gauge theories called quantum double models[11, 54, 55], with gauge group Z_2. However, the low-energy effective theory for Kitaev model in the limit $J_z \gg J_x, J_y$ is a toric-code-type model defined on the diamond lattice[5, 52], which is not a quantum double model. This is because, even though this effective Hamiltonian is a sum of plaquette operators B_p, each of the three sigma matrices at a particular site is part of some B_p, thus B_p's cannot be considered as the plaquette operators in a Z_2 quantum double model, which

are products of the same type of sigma matrix at different links. Consequently, we cannot apply the general result for TEE for quantum double models to our model.

Then the question remains whether TEE being $\ln 2$ for 3D Kitaev model is a coincidence or due to some underlying Z_2 gauge structure. To answer this we need to further explore the general relations among topological entanglement entropy, gauge group and total quantum dimension in three dimensions.

Chapter 4

Zero Energy Majorana Edge Modes

In topologically ordered systems, robust gapless states localized at the boundary encode information about the topology of the bulk [3, 12, 14, 13, 61]. In general, the number of such edge states is related to bulk topological invariants. The most well-known example of topological edge states is in quantum Hall systems [15, 16, 17, 18].

So far, most of the work on explicit calculation of edge states has been done for two dimensional systems. In 3D, edge states have been obtained for tight-binding model for complex fermions on the hyperhoneycomb lattice [62, 63]. In this paper we do a detailed analysis of the edge states in the 3D Kitaev model. We obtain analytical solutions for the gapless Majorana edge modes for three different geometries for the edges (zigzag, bearded, and armchair). We also find the parameter regimes in which each type of edge mode exists.

Zero-energy edge states exist in both gapped and gapless phases. In the gapless phase, the gap between the filled negative energy band and the empty postive energy band vanishes along a line in the $\mathbf{k}$-space, which corresponds to a nodal-line semimetal. Nodal lines in general give rise to topologically robust zero-energy surface bands with flat dispersion, known as drumhead states [64, 65, 66, 63]. Such states in 3D Kitaev models have been explored in Refs. [67, 68, 69]. In this paper we obtain explicit solutions for these drumhead states.

For the tight-binding model for complex fermions on the honeycomb lattice, the bulk spectrum and the edge states [70, 71] are identical to that of the Kitaev model, if a particular choice of the hopping amplitude is made based on the coupling parameters of the Kitaev model. Similar correspondence exists in 3D also, as we show later. We explain this equivalence through a correspondence between noninteracting Majorana fermion and complex fermion Hamiltonians, which exists only when sublattice symmetry is present.

In this chapter we present our results on zero-energy edge states in the 3D Kitaev model. In Sec. 4.2 we obtain the edge modes for various geometries and find the conditions for

the existence of each type of edge mode and the corresponding parameter regime. In Sec. 4.3 we show the correspondence between Majorana modes and complex fermion modes on bipartite lattices.

4.1 Bulk energy spectrum

Kitaev Hamiltonian in **k**-space has the form [see Eq. (4.1)] $H = \sum_{\mathbf{k}} \phi_{\mathbf{k}}^\dagger H_{\mathbf{k}} \phi_{\mathbf{k}}$, where $\phi_{\mathbf{k}}^\dagger = \begin{bmatrix} a_{\mathbf{k}}^\dagger & c_{\mathbf{k}}^\dagger & b_{\mathbf{k}}^\dagger & d_{\mathbf{k}}^\dagger \end{bmatrix}$ and

$$H_{\mathbf{k}} = i \begin{bmatrix} 0 & h_{\mathbf{k}} \\ -h_{\mathbf{k}}^\dagger & 0 \end{bmatrix}, \tag{4.1}$$

with

$$h_{\mathbf{k}} = 2 \begin{bmatrix} J_z e^{ik_z} & J_x e^{-ik_x} + J_y e^{ik_x} \\ J_x e^{-ik_y} + J_y e^{ik_y} & J_z e^{ik_z} \end{bmatrix}. \tag{4.2}$$

The diagonal blocks of $H_{\mathbf{k}}$ are zero due to the sublattice symmetry: the lattice is bipartite and therefore there is no hopping between sites belonging to the same sublattice. Here A and C sites are in odd sublattice and B and D sites are in even sublattice.

Sublattice symmetry implies that

$$H_{\mathbf{k}} \Gamma = -\Gamma H_{\mathbf{k}}, \tag{4.3}$$

where

$$\Gamma = \begin{bmatrix} \mathbb{1} & 0 \\ 0 & -\mathbb{1} \end{bmatrix}.$$

(In the above $\mathbb{1}$ is the 2×2 identity matrix.) Therefore, if $\psi_{\mathbf{k}}$ is an eigenvector of $H_{\mathbf{k}}$ with eigenvalue $E_{\mathbf{k}}$, then $\Gamma\psi_{\mathbf{k}}$ will be an eigenvector with eigenvalue $-E_{\mathbf{k}}$. Writing

$$\psi_{\mathbf{k}} = \begin{bmatrix} \psi_{\mathbf{k},1} \\ \psi_{\mathbf{k},2} \end{bmatrix},$$

where $\psi_{\mathbf{k},1}$ and $\psi_{\mathbf{k},2}$ are two-component wave functions, the eigenvalue equation becomes

$$ih_{\mathbf{k}}\psi_{\mathbf{k},2} = E_{\mathbf{k}}\psi_{\mathbf{k},1} \tag{4.4}$$

$$-ih_{\mathbf{k}}^{\dagger}\psi_{\mathbf{k},1} = E_{\mathbf{k}}\psi_{\mathbf{k},2} \tag{4.5}$$

Then,

$$(h_{\mathbf{k}}h_{\mathbf{k}}^{\dagger})\psi_{\mathbf{k},1} = E_{\mathbf{k}}^2\psi_{\mathbf{k},1}, \tag{4.6}$$

$$(h_{\mathbf{k}}^{\dagger}h_{\mathbf{k}})\psi_{\mathbf{k},2} = E_{\mathbf{k}}^2\psi_{\mathbf{k},2} \tag{4.7}$$

Solving the above eigenvalue equations, we get

$$\begin{aligned} E^2(\mathbf{k}) = 4\left[J_x^2 + J_y^2 + J_z^2 + 2J_xJ_y\cos(k_x+k_y)\cos(k_y-k_x)\right] \pm 4\Bigg\{ & J_x^2J_y^2 + 2J_x^2J_z^2 + 2J_y^2J_z^2 \\ & + 2J_xJ_yJ_z^2\Big[2\cos(k_x+k_y)\cos(k_y-k_x) + \cos(k_x-k_y+2k_z) + \cos(k_x-k_y-2k_z)\Big] \\ & + J_x^2J_y^2\Big[\cos 2(k_x+k_y)\cos 2(k_x-k_y) - \cos 2(k_x+k_y) - \cos 2(k_x-k_y)\Big] \\ & + 2J_x^2J_z^2\cos(k_x+k_y+2k_z) + 2J_y^2J_z^2\cos(k_x+k_y-2k_z)\Bigg\}^{1/2}. \end{aligned} \tag{4.8}$$

For the spectrum to be gapless, $E(\mathbf{k})$ should vanish for some $\mathbf{k}$, i.e., $(h_{\mathbf{k}}h_{\mathbf{k}}^{\dagger})\psi_{\mathbf{k},1} = 0$. This implies that $|h_{\mathbf{k}}\psi_{\mathbf{k},1}|^2 = 0$, which in turn leads to $h_{\mathbf{k}}\psi_{\mathbf{k},1} = 0$. This gives the condition $\det h_{\mathbf{k}} = 0$, which, using $h_{\mathbf{k}}$ given in Eq. (4.2), becomes

$$J_z^2\, e^{i2k_z} - (J_xe^{-ik_x} + J_ye^{ik_x})(J_xe^{-ik_y} + J_ye^{ik_y}) = 0. \tag{4.9}$$

The above condition can be satisfied for at least some $\mathbf{k}$ only when

$$\big||J_y| - |J_x|\big| \le |J_z| \le \big||J_y| + |J_x|\big|. \tag{4.10}$$

This is equivalent to the triangle inequalities among $|J_x|, |J_y|, |J_z|$. In Fig. 4.1 the shaded regions correspond to the gapless phase, when $J_z = 1$

When Inequality (4.10) is satisfied, $E(\mathbf{k})$ vanishes along a loop in $\mathbf{k}$-space determined by Eq. (4.9) and the dispersion is linear in $|\mathbf{k}|$ away from the gapless loop [5].

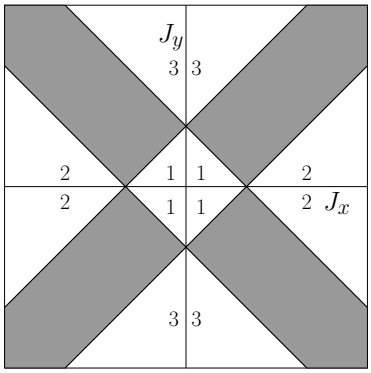

Figure 4.1: Phase diagram in $J_x - J_y$ space with $J_z = 1$. The bulk spectrum is gapless in the shaded regions and gapped elsewhere.

4.1.1 Symmetries

The Kitaev Hamiltonian on the hyperhoneycomb lattice [Eq. (2.21)] has the following symmetries:

1. Under spatial reflection about an x-z plane followed by another reflection about a y-z plane, $J_x \leftrightarrow J_y$ and J_z is invariant.

2. Rotate spins on one of the sublattices (either $[A, C]$ or $[B, D]$) about the z-axis by π. Then $\sigma_x \to -\sigma_x$, $\sigma_y \to -\sigma_y$ and $\sigma_z \to \sigma_z$ on the rotated sublattice. Under this transformation, $J_x \to -J_x$, $J_y \to -J_y$ while J_z is invariant.

3. Rotate spins on alternate x-y planes about the x-axis by π. Then $\sigma_x \to \sigma_x$, $\sigma_y \to -\sigma_y$ and $\sigma_z \to -\sigma_z$. Since z-links connect sites in neighbouring planes and x- and y- links are in-plane, under this transformation, $J_z \to -J_z$ while J_x and J_y are invariant.

It is easy to verify that the above symmeties are manifest in the energy spectrum given in Eq. (4.8). [For the first symmetry transformation, we will have to transform $\mathbf{k}$ also ($k_z \to -k_z$) to leave $E(\mathbf{k})$ invariant.]

The above symmetries mean that in the $J_x - J_y$ plane we can restrict ourselves to the region between angles $-\pi/4$ and $\pi/4$ (with respect to positive J_x direction). However, for aesthetic reasons we show the full plane in the phase diagaram.

4.2 Zero-energy edge modes

In this section we obtain the solutions of zero-energy modes localized at the boundaries. For this we apply periodic boundary conditions in two of the directions and leave the remaining direction open.

Let $\gamma = \sum_{\mathbf{r}} [\psi_{\mathbf{r}} a_{\mathbf{r}} + \phi_{\mathbf{r}} b_{\mathbf{r}} + \chi_{\mathbf{r}} c_{\mathbf{r}} + \tau_{\mathbf{r}} d_{\mathbf{r}}]$ be a zero-energy mode, where $\psi_{\mathbf{r}}, \phi_{\mathbf{r}}, \chi_{\mathbf{r}}$ and $\tau_{\mathbf{r}}$ are the wave functions corresponding to the four sites within the unit cell. Then the Heisenberg equation of motion gives

$$d\gamma/dt = [H, \gamma] = 0. \tag{4.11}$$

We now obtain solutions for the above equation for different types of edges, which are not related by any lattice symmetries and are truly distinct. We find that the zero-energy modes are localized at either of the sublattices depending on the type of the edge.

4.2.1 Zigzag edge

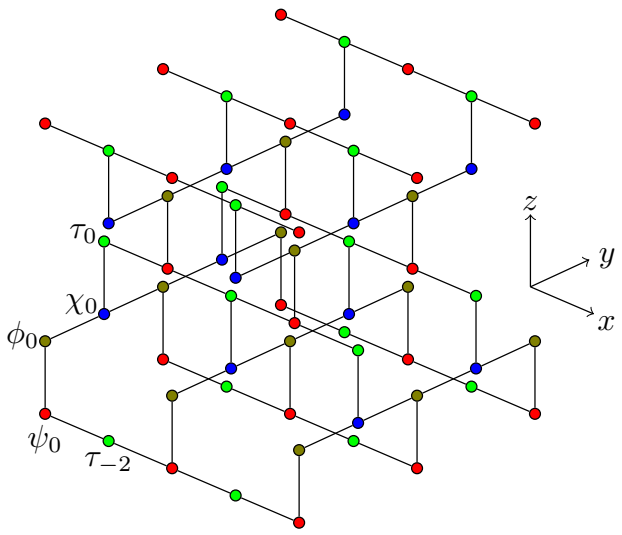

Figure 4.2: Zigzag edge at the bottom. Periodic boundary condition is imposed in the x- and y- directions.

We first consider the edge shown in Fig.4.2. This is analogous to the zigzag edge for the honeycomb lattice [72, 71, 73] and we shall also call it a zigzag edge, even though the zigzag structure in the hyperhoneycomb lattice has been smoothed out in our depiction of the lattice.

We impose periodic boundary condition in x- and y- directions, keeping the z-direction open. Then it is more convenient to use unit vectors in x- y- and z- directions as bases to write the lattice vector:

$$\mathbf{r} = m\hat{\mathbf{x}} + n\hat{\mathbf{y}} + p\hat{\mathbf{z}}.$$

Here p takes even integer values; when $p = 0, 4, 8, \cdots$, m and n take only even integer values, and when $p = 2, 6, 10, \cdots$, m and n are both odd. Then we can choose plane wave solutions in x- and y- directions and thus write the wave functions as

$$\begin{aligned} \psi_{m,n,p} &= e^{ik_x m} e^{ik_y n} \psi_p \\ \phi_{m,n,p} &= e^{ik_x m} e^{ik_y n} \phi_p \\ \chi_{m,n,p} &= e^{ik_x m} e^{ik_y n} \chi_p \\ \tau_{m,n,p} &= e^{ik_x m} e^{ik_y n} \tau_p \end{aligned} \tag{4.12}$$

where $k_x = (\pi q/L_x),\ k_y = (\pi s/L_y)$, with q and s taking integer values, and L_x and L_y are the number of unit cells in the x- and y- directions, respectively. The equation of motion (4.11) then becomes

$$J_1 \tau_{p-2} + J_z \phi_p = 0, \tag{4.13}$$

$$-J_x \phi_p - J_y e^{2ik_y} \phi_p - J_z \tau_p = 0, \tag{4.14}$$

$$-J_y e^{-2ik_y} \chi_p - J_z \psi_p - J_x \chi_p = 0, \tag{4.15}$$

$$J_z \chi_p + J_2 \psi_{p+2} = 0, \tag{4.16}$$

where

$$J_1 = J_x e^{-i(k_x + k_y)} + J_y e^{i(k_x - k_y)} = J_2^*. \tag{4.17}$$

Note that, because of the sublattice symmetry, the Eqs. (4.13) and (4.14) involve only ϕ and τ, and Eqs. (4.15) and (4.16) involve only ψ and χ. After decoupling the equations we obtain

$$\begin{aligned} \psi_p &= \lambda \psi_{p+2},\ \ \phi_p = \lambda \phi_{p-2}, \\ \chi_p &= \lambda \chi_{p+2},\ \ \tau_p = \lambda \tau_{p-2}, \end{aligned} \tag{4.18}$$

where

$$\lambda = \frac{(J_x^2 + J_y^2 + 2J_xJ_y\cos 2k_x)^{\frac{1}{2}}(J_x^2 + J_y^2 + 2J_xJ_y\cos 2k_y)^{\frac{1}{2}}}{J_z^2} \tag{4.19}$$

We assign the value $p = 0$ to the bottom-most unit cells that lie entirely within the lattice (Fig. 4.2). This gives rise to the following boundary conditions:

$$\begin{aligned} \psi_0 &= 0, \\ \chi_{-2} &= 0, \end{aligned} \tag{4.20}$$

In the limit $L_z \to \infty$,

$$\begin{aligned} \psi_p &= 0, \\ \phi_p &= \lambda^{p/2}\phi_0, \\ \chi_p &= 0, \\ \tau_p &= \lambda^{(p/2+1)}\tau_{-2}, \end{aligned} \tag{4.21}$$

is a solution of Eqs. (4.18) satisfying the above boundary conditions, provided $\lambda < 1$. This corresponds to an edge mode localized at the bottom and decaying exponentially, and having nonvanishing amplitude only at B and D sites.

4.2.2 Bearded edge

Bearded edge is shown in Fig. 4.3. In this case the boundary conditions are

$$\begin{aligned} \phi_0 &= 0, \\ \tau_{-2} &= 0. \end{aligned} \tag{4.22}$$

When $\lambda > 1$, we obtain the following solution to Eqs. (4.18) consistent with the above boundary conditions:

$$\begin{aligned} \psi_p &= \left(\frac{1}{\lambda}\right)^{p/2}\psi_0, \\ \phi_p &= 0, \\ \chi_p &= \left(\frac{1}{\lambda}\right)^{p/2}\chi_0, \\ \tau_p &= 0. \end{aligned} \tag{4.23}$$

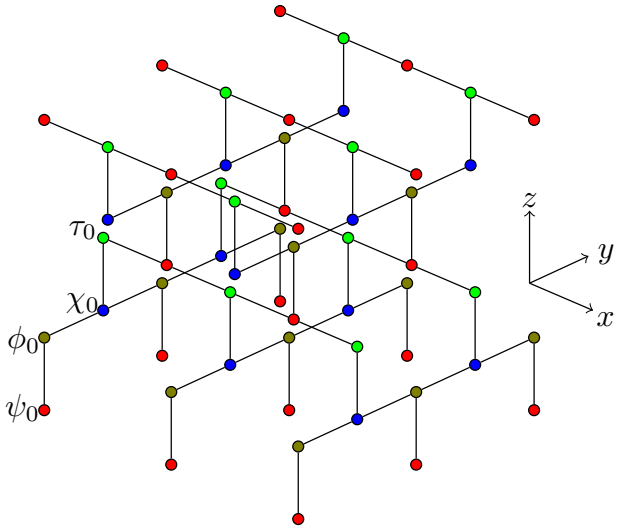

Figure 4.3: Bearded edge at the bottom. Periodic boundary condition is imposed in the x- and y- directions.

This solution is also localized at the bottom with an exponentially decaying wave function, but has nonvanishing amplitude only at A and C sites.

4.2.3 Armchair edge

Another type of edge can be formed by cutting the lattice perpendicular to the x- (or y-) direction as shown in Fig. 4.4. The edge thus obtained is analogous to the armchair edge for honeycomb lattice and we also retain the same name. Applying periodic boundary conditions in y- and z- directions, the solution takes plane wave form in the respective coordinates:

$$\begin{aligned} \psi_{m,n,p} &= e^{ik_y n} e^{ik_z p} \psi_m \\ \phi_{m,n,p} &= e^{ik_y n} e^{ik_z p} \phi_m \\ \chi_{m,n,p} &= e^{ik_y n} e^{ik_z p} \chi_m \\ \tau_{m,n,p} &= e^{ik_y n} e^{ik_z p} \tau_m \end{aligned} \tag{4.24}$$

where $k_y = (\pi q/L_y)$, $k_z = (\pi s/2L_z)$, q, s take integer values, and L_y and L_z are the number of unit cells in y and z directions, respectively. Then the equation of motion for

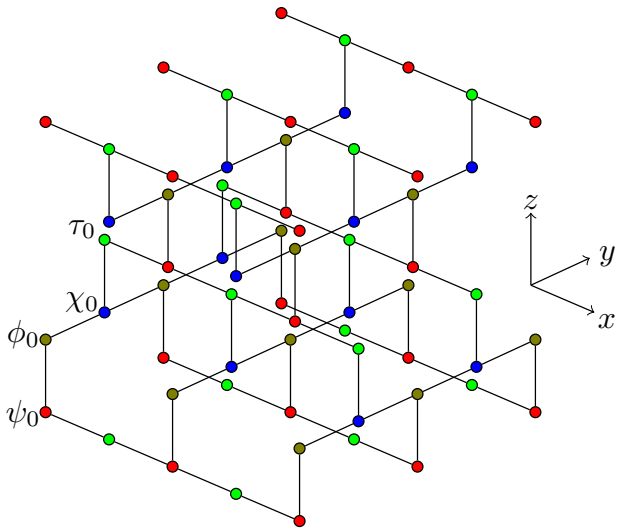

Figure 4.4: Armchair edge obtained by cutting the lattice along a plane normal to the x-axis. Periodic boundary condition is imposed in y- and z- directions.

zero modes [Eqs. (4.11)] becomes

$$\alpha(J_y\psi_{m-1} + J_x\psi_{m+1}) + J_z\chi_m = 0, \tag{4.25}$$

$$J_1^*\chi_m + J_z\psi_m = 0, \tag{4.26}$$

$$\alpha^*\left(J_x\tau_{m-1} + J_y\tau_{m+1}\right) + J_z\phi_m = 0, \tag{4.27}$$

$$J_1\phi_m + J_z\tau_m = 0, \tag{4.28}$$

where $\alpha = e^{ik_y}e^{i2k_z}$, and $J_1 = (J_x + J_y e^{i2k_z})$. We can use Eq. (4.26) to eliminate χ from Eq. (4.25); similarly, Eq. (4.28) can be used to eliminate ϕ from Eq. (4.27). Then we obtain

$$\alpha J_1^*(J_y\psi_{m-1} + J_x\psi_{m+1}) = J_z^2\psi_m, \tag{4.29}$$

$$\chi_m = -\frac{J_z}{J_1^*}\psi_m, \tag{4.30}$$

$$\alpha^* J_1(J_x\tau_{m-1} + J_y\tau_{m+1}) = J_z^2\tau_m, \tag{4.31}$$

$$\phi_m = -\frac{J_z}{J_1}\tau_m, \tag{4.32}$$

Equation (4.29) can be solved by the substitution $\psi_m = x^m$, and we obtain $x = x_\pm$, where

$$x_\pm = \frac{J_z^2 \pm \sqrt{J_z^4 - 4\alpha^2 (J_1^*)^2 J_x J_y}}{2\alpha J_1^* J_x} \tag{4.33}$$

Similarly, Eq. (4.31) can be solved by trying $\tau_m = y^m$, and we get $y = y_\pm$, where

$$y_\pm = \frac{J_z^2 \pm \sqrt{J_z^4 - 4(\alpha^*)^2 {J_1}^2 J_x J_y}}{2\alpha^* J_1 J_y} \tag{4.34}$$

Then the general solution for ψ and τ can be written as

$$\psi_m = A x_+^m + B x_-^m, \tag{4.35}$$

$$\tau_m = C y_+^m + D y_-^m. \tag{4.36}$$

with χ and ϕ given by Eqs. (4.30) and (4.32), respectively.

In our case the boundary conditions are $\psi_{-1} = 0$, and $\tau_{-1} = 0$. Applying these, we obtain the following two independent solutions:

$$\begin{aligned} \psi_m &= \left(\frac{x_+^{m+1} - x_-^{m+1}}{x_+ - x_-} \right) \psi_0, \\ \chi_m &= -\frac{J_z}{J_1^*} \psi_m, \\ \phi_m &= 0, \\ \tau_m &= 0, \end{aligned} \tag{4.37}$$

and

$$\begin{aligned} \tau_m &= \left(\frac{y_+^{m+1} - y_-^{m+1}}{y_+ - y_-} \right) \tau_0, \\ \phi_m &= -\frac{J_z}{J_1} \tau_m, \\ \psi_m &= 0, \\ \chi_m &= 0. \end{aligned} \tag{4.38}$$

In the limit $L_x \to \infty$, Solution (4.37), which is nonvanishing only at A and C sites, exists when $|x_\pm| < 1$. Similarly, Solution (4.38), which is nonvanishing only at B and D sites, exists when $|y_\pm| < 1$.

Edge type	Region-1	Region-2	Region-3
Zigzag	[B, D]	x	x
Bearded	x	[A, C]	[A, C]
Armchair	x	[A, C]	[B, D]

Table 4.1: Edge states in different regions of the gapped phase shown in the phase diagram (Fig. 4.1). [.., ..] denotes the types of sites at which the wave function is nonvanishing

Noting that

$$x_+ x_- = \frac{J_y}{J_x} \text{ and } y_+ y_- = \frac{J_x}{J_y},$$

only one of the two solutions can exist at a time: Solution (4.37) when $J_x > J_y$, and Solution (4.38) when $J_x < J_y$. Interestingly, neither solution exists when $J_x = J_y$.

4.2.4 Existence of edge modes and phase diagram

We will now explore the phase diagram and find out in which regions a particular type of edge mode exists. We rescale the coupling parameters J_x and J_y with J_z (i.e., put $J_z = 1$).

Existence of edge modes for zigzag and bearded edges depends on whether the parameter λ [Eq. (4.19)] is less than 1 or greater than 1. Maximum value of λ with respect to $\mathbf{k}$ is $\lambda_{max} = |J_x| + |J_y|$, and the minimum value is $\lambda_{min} = ||J_x| - |J_y||$.

For the existence of zigzag edge mode, $\lambda < 1$. This condition will be satisfied for all values of $\mathbf{k}$ if $\lambda_{max} < 1$, i.e., $|J_x| + |J_y| < 1$. This corresponds to Region 1 in the phase diagram shown in Fig. 4.1, which is gapped. The condition for λ to be less than 1 for some $\mathbf{k}$ is $\lambda_{min} < 1$. This condition is satisfied in the gapless region (shaded area in the figure). In the gapped Regions 2 and 3, $\lambda_{min} > 1$ and there are no zigzag edge modes.

The bearded edge modes exist when $\lambda > 1$. This condition will be satisfied for all values of $\mathbf{k}$ if $\lambda_{min} > 1$, i.e., $||J_x| - |J_y|| > 1$ and it corresponds to gapped Regions 2 and 3. In the gapless region the existence condition will hold for some values of $\mathbf{k}$, and no bearded edge mode exists in Region 1.

Finally, for the armchair edge, as shown in Appendix B, Solution (4.37) exists for all $\mathbf{k}$ in Region 2 whereas Solution (4.38) exists for all $\mathbf{k}$ in Region 3. In the gapless phase, for a subset of $\mathbf{k}$ values, Solution (4.37) exists in the region where $|J_x| > |J_y|$ and Solution (4.38) exists in the region where $|J_y| > |J_x|$.

To summarize, in the gapless phase all three types of edge modes exist for a subset of

$\mathbf{k}$ values. Each type of solution exists only in some part of the gapped phase, but in that region all values of $\mathbf{k}$ have corresponding solutions.

Table 4.1 shows the gapped regions in the phase diagram in which a particular type of edge mode admits solutions. As we can notice, in a given region not all types of edges result in gapless edge states. To understand this we first note that in Region-1 z-type bonds are the strongest, in Region-2 x-type, and in Region-3 y-type. For a given type of edge, the gapeless edge states will be localized around those boundary sites that are *not* linked to another site via a strong bond. This can be readily seen in the case of Su-Schrieffer-Heeger model [74] and Kitaev chain [26] and the honeycomb lattice Kitaev model [73].

For the zig-zag edge such weakly-linked boundary sites exist only when the z-type bonds are the strongest, and they are D-type (Fig. 4.2). The edge states are localized around these sites and thus have nonvanishing amplitudes only at B and D sites.

For both bearded and armchair edges, weakly-linked boundary sites exist only when the strongest bonds are either x-type (Region 2) or y-type (Region 3). For bearded edge in both the regions such sites are A-type and the edge states will then have nonvanishing amplitudes only at A and C sites (Fig. 4.3). As for the armchair edge, in Region 2 the weakly-linked boundary sites are A-type and in Region 3 D-type (Fig. 4.4), and the corresponding edge state wave functions are nonvanishing only at $[A, C]$ sites and $[B, D]$ sites, respectively.

4.2.5 Drumhead states

As we have found above, in the gapless phase zero-energy edge modes exist only for a subset of momentum values along the boundary surface. We now argue that these states are precisely the drumhead surface states arising from nodal-lines [65, 69]. Such states can be understood as follows: to each value of surface momentum [(k_x, k_y), if the boundary is normal to the z-direction] we can associate a winding number, which is a $\mathbf{k}$-space integral over a line along the direction normal to the surface [65]. The winding number, being a topological invariant, will have one value for all lines going through the gapless contour and another value for all lines lying outside the contour. One of these values will be nontrivial and then there will be zero-energy surface states corresponding to those momenta (since vacuum is topologically trivial and there must exist gapless modes at the interface). The upshot is there will be zero-energy states corresponding to surface momenta lying either inside or outside the contour obtained by projecting the gapless contour on to the appropriate Brillouin zone boundary.

For the hyperhoneycomb lattice Kitaev model the condition for the gap to vanish, given

in Eq. (4.10), can be written as

$$J_z^2\, e^{i2k_z} = (J_x e^{-ik_x} + J_y e^{ik_x})(J_x e^{-ik_y} + J_y e^{ik_y}). \tag{4.39}$$

Equating the modulus of each side of the above equation, we obtain the following condition involving only k_x and k_y:

$$J_z^2 = (J_x^2 + J_y^2 + 2J_xJ_y\cos 2k_x)^{\frac{1}{2}}(J_x^2 + J_y^2 + 2J_xJ_y\cos 2k_y)^{\frac{1}{2}}. \tag{4.40}$$

Equating the phases will give a second condition involving all three components of momenta, but the above equation gives the projection of the gapless contour on to any constant k_z plane.

For zigzag and bearded edges the boundary surface is parallel to the $x-y$ plane, thus the projection of the gapless countour on to the Brillouin zone boundary is given by Eq. (4.40) itself. This is precisely the equation obtained by putting $\lambda = 1$ in Eq. (4.19). For zigzag egde, the existence condition for edge state is $\lambda < 1$, which is satisfied in the interior of the projection of the gapless countour. Similarly, for the bearded edge the existence condition for edge states is $\lambda > 1$, which is satisfied in the exterior of the projected contour. This confirms that the edge state solutions we have obtained for zigzag and bearded edges in the gapless phase are indeed drumhead states.

For the armchair edge we need the projection of the gapless contour on to the $k_y - k_z$ plane, which is not easily tractable analytically.

4.3 Correspondence between Majorana modes and fermion modes on bipartite lattices

In two dimensions, the bulk spectrum and the zero-energy edge modes for the Kitaev model [4, 73] and complex fermion tight-binding model [70, 71] are identical if we choose the hopping amplitude between two sites in the latter to be twice the coupling constant in the Kitaev model.

Tight-binding model for complex fermions has been studied on the hyperhoneycomb lattice[62] and it is straightforward to derive the bulk spectrum. For the choice $t_{ij} = 2J_{\alpha_{ij}}$, we get exactly the same dispersion as that of Kitaev model given in Eq. (4.8).

Similarly, the zigzag and the bearded edge zero modes we have derived in this paper are also in agreement with those for the complex fermion tight-binding model obtained in

Ref. [63] (the armchair edge was not considered in this reference).

The above equivalence between Majorana normal modes in Kitaev model and the fermion normal modes in tight-binding model is quite striking and calls for an explanation. In the following we show a correspondence between noninteracting Majorana fermions and complex fermions that exists only when sublattice symmetry is present and which explains the above equivalence.

Consider the following tight-binding Hamiltonian

$$\hat{H}_F = \sum_{ij} t_{ij} c_i^\dagger c_j, \tag{4.41}$$

where $c_i^\dagger$ and c_i are, respectively, the fermion creation and annihilation operators at site i. We further assume that t_{ij} are real, then hermiticity of H_F demands that $t_{ij} = t_{ji}$. Let T denote the matrix with entries t_{ij}. Then the one-particle spectrum of H_F is given by the eigenvalues T.

Next we consider the following Majorana fermion Hamiltonian

$$\hat{H}_{MF} = \frac{i}{4} \sum_{ij} t'_{ij} b_i b_j, \tag{4.42}$$

where b_i are Majorana operators [$b_i^\dagger = b_i,\ \{b_i, b_j\} = 2\delta_{ij}$]. In this case hermiticity demands that $t'_{ij} = -t'_{ji}$. The one-particle spectrum for the above Hamiltonian is given by the eigenvalues of the matrix T', whose entries are t'_{ij} [4].

If we take $t_{ii} = 0$, then there is a natural one-to-one mapping between H_F and H_{MF}: $t'_{ij} = t_{ij}$ for $j > i$ and $t'_{ij} = -t_{ij}$ for $j < i$. In general the matrices t_{ij} and t'_{ij} thus related will have different eigenvalues and eigenvectors. However, as we will show next, the two matrices have identical eigenvalues and eigenvectors when the lattice is bipartite and the Hamiltonian has sublattice symmetry.

Let A and B denote the two sublattices. Then sublattice symmetry implies that $t_{ij} \neq 0$ only when i and j are in different sublattices (in particular, $t_{ii} = 0$). After labeling the sites so that all sites in each sublattice are grouped together, the matrices T and T' take the form

$$T = \begin{bmatrix} 0 & h \\ h^\dagger & 0 \end{bmatrix}, \tag{4.43}$$

$$T' = \begin{bmatrix} 0 & ih \\ -ih^\dagger & 0 \end{bmatrix}, \tag{4.44}$$

where the nonvanishing off-diagonal blocks contain the hopping amplitudes between the two sublattices. Let (Ψ_A, Ψ_B) denote the eigenvector of T with eigenvalue E:

$$\begin{bmatrix} 0 & h \\ h^\dagger & 0 \end{bmatrix} \begin{bmatrix} \Psi_A \\ \Psi_B \end{bmatrix} = E \begin{bmatrix} \Psi_A \\ \Psi_B \end{bmatrix}. \tag{4.45}$$

Then

$$\begin{aligned} (hh^\dagger)\Psi_A &= E^2 \Psi_A, \\ (h^\dagger h)\Psi_B &= E^2 \Psi_B. \end{aligned} \tag{4.46}$$

Similarly, let (Φ_A, Φ_B) denote the eigenvector of T' with eigenvalue E':

$$\begin{bmatrix} 0 & ih \\ -ih^\dagger & 0 \end{bmatrix} \begin{bmatrix} \Phi_A \\ \Phi_B \end{bmatrix} = E' \begin{bmatrix} \Phi_A \\ \Phi_B \end{bmatrix}. \tag{4.47}$$

Then

$$\begin{aligned} (hh^\dagger)\Phi_A &= E'^2 \Phi_A, \\ (h^\dagger h)\Phi_B &= E'^2 \Phi_B. \end{aligned} \tag{4.48}$$

Therefore, we have the same eigenvalue equations [Eqs. (4.46) and (4.48)] in both the cases. In other words, the eigenmodes and eigenvalues of noninteracting complex fermions and Majorana fermions on a bipartite lattice, with hopping matrices of the form given in Eqs. (4.43) and (4.44) respectively, are identical. It is for this reason that the bulk spectrum and the gapless edge modes in Kitaev model and tight-binding model for complex fermions on the bipartite honeycomb and hyperhoneycomb lattices are identical.

We further note that the above correspondence is not the canonical mapping between a Majorana Hamiltonian and a complex fermion Hamiltonian obtained by writing each fermion mode in terms of two Majorana modes, in which case the number of Majorana modes will be double that of fermion modes and then both systems will obviously have the same energy spectrum. Then, the two Hamiltonians will be defined on different lattices—if we insist on one mode per site—since two sites in the Majorana model will correspond to a single site in the complex fermion model.

However, what we have established above is a correspondence between Majorana fermions and complex fermions on the same lattice, i.e., the number of Majorana modes is the same as that of complex fermion modes.

4.4 Summary

To summarize, we have obtained exact analytical solutions for gapless Majorana edge modes in the three dimensional Kitaev model. We have considered three types of edges: 1) zigzag, 2) bearded, and 3) armchair. When the bulk is gapped, each type of edge admits edge modes in some part of the phase diagram for all values of edge momentum $\mathbf{k}$.

However, throughout the gapless phase, for all three types of edges, edge states exist only for a subset of $\mathbf{k}$-values. For zigzag and bearded edges we have verified that these states are the drumhead surface states associated with nodal lines at the Fermi energy.

We have further established a general correspondence between noninteracting fermions and Majorana fermions on bipartite lattices, based on which we can understand the equivalence of their energy spectrum and eigenmodes.

Here we note that while obtaining the edge states for tight-binding model for complex fermions on hyperhoneycomb lattice, in Ref. [63] two of the three hopping amplitudes are taken to be equal, and only zigzag and bearded edges have been considered. As we have shown in Sec. 4.2.3, when two of the couplings are the same the armchair solutions do not exist. Thus, the solutions we have obtained for the armchair edge are new for the complex fermion case also.

Chapter 5

Summary and Discussion

In this thesis we have studied certain topological properties of the three-dimensional Kitaev model on a hyperhoneycomb lattice. We have calculated the topological entanglement entropy (TEE)and have also obtained exact solutions for zero-energy Majorana edge modes.

In the first part of the thesis, we have calculated TEE of the three-dimensional Kitaev model. We achieved this by first calculating the entanglement entropy of the ground state by extending a method introduced by Yao and Qi in the context the two-dimensional Kitaev model and then extracting TEE using a partitioning scheme that eliminates contributions to the entropy arising from local correlations. We found that that γ_0, the part of the TEE proportional to b_0 (zeroth Betti number), is $\ln 2$ and γ_1, the part of the TEE proportional to b_1 (first Betti number), is zero. We also found that for our model, TEE is not directly determined by the total quantum dimension of the system. The quantum dimension D of the model is $\sqrt{2}$, therefore $\gamma_0 \neq \ln D$. This is in contrast to general two-dimensional systems and many three- dimensional models, where TEE is directly given by the total quantum dimension. Our calculation also provides TEE for a three-dimensional toric code that emerges as the effective low energy theory for the Kitaev model in a particular limit.

In the second part of the thesis, we have obtained exact analytical solutions for gapless Majorana edge modes in the same model. We have considered three types of edges: (1) zigzag, (2) bearded, and (3) armchair, and found the regions in parameter space where each type of edge mode exists. We observed that when the bulk is gapped, each type of edge admits edge modes in some part of the phase diagram for all values of edge momentum $\mathbf{k}$. While the bulk is gapless, the edge states exist only for the subset of $\mathbf{k}$ values for all three types of edges. We have verified that these states are the drumhead surface states associated with the nodal line semimetals for zigzag and bearded edges. Furthermore, we have established a general correspondence between noninteracting fermion and Majorana fermions on a bipartite lattice with sublattice symmetry, which explains the equivalence of

energy spectrum and eigenmodes of Kitaev model and corresponding tight-binding model for complex fermion on the same lattice.

Bibliography

[1] X. G. Wen, F. Wilczek, and A. Zee, "Chiral spin states and superconductivity," *Phys. Rev. B*, vol. 39, pp. 11 413–11 423, Jun 1989. [Online]. Available: https://link.aps.org/doi/10.1103/PhysRevB.39.11413

[2] D. J. Thouless, M. Kohmoto, M. P. Nightingale, and M. den Nijs, "Quantized hall conductance in a two-dimensional periodic potential," *Phys. Rev. Lett.*, vol. 49, pp. 405–408, Aug 1982. [Online]. Available: https://link.aps.org/doi/10.1103/PhysRevLett.49.405

[3] M. Z. Hasan and C. L. Kane, "Colloquium: Topological insulators," *Rev. Mod. Phys.*, vol. 82, pp. 3045–3067, Nov 2010. [Online]. Available: https://link.aps.org/doi/10.1103/RevModPhys.82.3045

[4] A. Kitaev, "Anyons in an exactly solved model and beyond," *Annals of Physics*, vol. 321, no. 1, pp. 2 – 111, 2006, january Special Issue. [Online]. Available: http://www.sciencedirect.com/science/article/pii/S0003491605002381

[5] S. Mandal and N. Surendran, "Exactly solvable kitaev model in three dimensions," *Phys. Rev. B*, vol. 79, p. 024426, Jan 2009. [Online]. Available: https://link.aps.org/doi/10.1103/PhysRevB.79.024426

[6] M. A. Nielsen and I. L. Chuang, *Quantum Computation and Quantum Information: 10th Anniversary Edition*, 10th ed. New York, NY, USA: Cambridge University Press, 2011.

[7] P. Calabrese and J. Cardy, "Entanglement entropy and conformal field theory," *Journal of Physics A: Mathematical and Theoretical*, vol. 42, no. 50, p. 504005, 2009. [Online]. Available: http://stacks.iop.org/1751-8121/42/i=50/a=504005

[8] ——, "Entanglement entropy and quantum field theory," *Journal of Statistical Mechanics: Theory and Experiment*, vol. 2004, no. 06, p. P06002, 2004. [Online]. Available: http://stacks.iop.org/1742-5468/2004/i=06/a=P06002

[9] A. Kitaev and J. Preskill, "Topological entanglement entropy," *Phys. Rev. Lett.*, vol. 96, p. 110404, Mar 2006. [Online]. Available: https://link.aps.org/doi/10.1103/PhysRevLett.96.110404

[10] M. Levin and X.-G. Wen, "Detecting topological order in a ground state wave function," *Phys. Rev. Lett.*, vol. 96, p. 110405, Mar 2006. [Online]. Available: https://link.aps.org/doi/10.1103/PhysRevLett.96.110405

[11] T. Grover, A. M. Turner, and A. Vishwanath, "Entanglement entropy of gapped phases and topological order in three dimensions," *Phys. Rev. B*, vol. 84, p. 195120, Nov 2011. [Online]. Available: https://link.aps.org/doi/10.1103/PhysRevB.84.195120

[12] X.-L. Qi and S.-C. Zhang, "Topological insulators and superconductors," *Rev. Mod. Phys.*, vol. 83, pp. 1057–1110, Oct 2011. [Online]. Available: https://link.aps.org/doi/10.1103/RevModPhys.83.1057

[13] A. P. Schnyder, S. Ryu, A. Furusaki, and A. W. W. Ludwig, "Classification of topological insulators and superconductors in three spatial dimensions," *Phys. Rev. B*, vol. 78, p. 195125, Nov 2008. [Online]. Available: https://link.aps.org/doi/10.1103/PhysRevB.78.195125

[14] C. Nayak, S. H. Simon, A. Stern, M. Freedman, and S. Das Sarma, "Non-abelian anyons and topological quantum computation," *Rev. Mod. Phys.*, vol. 80, pp. 1083–1159, Sep 2008. [Online]. Available: https://link.aps.org/doi/10.1103/RevModPhys.80.1083

[15] K. v. Klitzing, G. Dorda, and M. Pepper, "New method for high-accuracy determination of the fine-structure constant based on quantized hall resistance," *Phys. Rev. Lett.*, vol. 45, pp. 494–497, Aug 1980. [Online]. Available: https://link.aps.org/doi/10.1103/PhysRevLett.45.494

[16] D. C. Tsui, H. L. Stormer, and A. C. Gossard, "Two-dimensional magnetotransport in the extreme quantum limit," *Phys. Rev. Lett.*, vol. 48, pp. 1559–1562, May 1982. [Online]. Available: https://link.aps.org/doi/10.1103/PhysRevLett.48.1559

[17] B. I. Halperin, "Quantized hall conductance, current-carrying edge states, and the existence of extended states in a two-dimensional disordered potential," *Phys. Rev. B*, vol. 25, pp. 2185–2190, Feb 1982. [Online]. Available: https://link.aps.org/doi/10.1103/PhysRevB.25.2185

[18] X. G. Wen, "Electrodynamical properties of gapless edge excitations in the fractional quantum hall states," *Phys. Rev. Lett.*, vol. 64, pp. 2206–2209, Apr 1990. [Online]. Available: https://link.aps.org/doi/10.1103/PhysRevLett.64.2206

[19] C. L. Kane and E. J. Mele, "Quantum spin hall effect in graphene," *Phys. Rev. Lett.*, vol. 95, p. 226801, Nov 2005. [Online]. Available: https://link.aps.org/doi/10.1103/PhysRevLett.95.226801

[20] B. A. Bernevig and S.-C. Zhang, "Quantum spin hall effect," *Phys. Rev. Lett.*, vol. 96, p. 106802, Mar 2006. [Online]. Available: https://link.aps.org/doi/10.1103/PhysRevLett.96.106802

[21] B. A. Bernevig, T. L. Hughes, and S.-C. Zhang, "Quantum spin hall effect and topological phase transition in hgte quantum wells," *Science*, vol. 314, no. 5806, pp. 1757–1761, 2006. [Online]. Available: http://science.sciencemag.org/content/314/5806/1757

[22] M. König, S. Wiedmann, C. Brüne, A. Roth, H. Buhmann, L. W. Molenkamp, X.-L. Qi, and S.-C. Zhang, "Quantum spin hall insulator state in hgte quantum wells," *Science*, vol. 318, no. 5851, pp. 766–770, 2007. [Online]. Available: http://science.sciencemag.org/content/318/5851/766

[23] L. Fu, C. L. Kane, and E. J. Mele, "Topological insulators in three dimensions," *Phys. Rev. Lett.*, vol. 98, p. 106803, Mar 2007. [Online]. Available: https://link.aps.org/doi/10.1103/PhysRevLett.98.106803

[24] R. Roy, "Topological phases and the quantum spin hall effect in three dimensions," *Phys. Rev. B*, vol. 79, p. 195322, May 2009. [Online]. Available: https://link.aps.org/doi/10.1103/PhysRevB.79.195322

[25] J. E. Moore and L. Balents, "Topological invariants of time-reversal-invariant band structures," *Phys. Rev. B*, vol. 75, p. 121306, Mar 2007. [Online]. Available: https://link.aps.org/doi/10.1103/PhysRevB.75.121306

[26] A. Y. Kitaev, "Unpaired majorana fermions in quantum wires," *Physics-Uspekhi*, vol. 44, no. 10S, pp. 131–136, oct 2001. [Online]. Available: https://doi.org/10.1070%2F1063-7869%2F44%2F10s%2Fs29

[27] L.-M. Duan, E. Demler, and M. D. Lukin, "Controlling spin exchange interactions of ultracold atoms in optical lattices," *Phys. Rev. Lett.*, vol. 91, p. 090402, Aug 2003. [Online]. Available: https://link.aps.org/doi/10.1103/PhysRevLett.91.090402

[28] A. Micheli, G. K. Brennen, and P. Zoller, "A toolbox for lattice-spin models with polar molecules," *Nature Physics*, vol. 2, pp. 341 EP –, Apr 2006, article. [Online]. Available: https://doi.org/10.1038/nphys287

[29] J. Q. You, X.-F. Shi, X. Hu, and F. Nori, "Quantum emulation of a spin system with topologically protected ground states using superconducting quantum circuits," *Phys. Rev. B*, vol. 81, p. 014505, Jan 2010. [Online]. Available: https://link.aps.org/doi/10.1103/PhysRevB.81.014505

[30] F. Wang, "Realization of the exactly solvable kitaev honeycomb lattice model in a spin-rotation-invariant system," *Phys. Rev. B*, vol. 81, p. 184416, May 2010. [Online]. Available: https://link.aps.org/doi/10.1103/PhysRevB.81.184416

[31] H.-C. Jiang, Z.-C. Gu, X.-L. Qi, and S. Trebst, "Possible proximity of the mott insulating iridate na_2iro_3 to a topological phase: Phase diagram of the heisenberg-kitaev model in a magnetic field," *Phys. Rev. B*, vol. 83, p. 245104, Jun 2011. [Online]. Available: https://link.aps.org/doi/10.1103/PhysRevB.83.245104

[32] J. Reuther, R. Thomale, and S. Trebst, "Finite-temperature phase diagram of the heisenberg-kitaev model," *Phys. Rev. B*, vol. 84, p. 100406, Sep 2011. [Online]. Available: https://link.aps.org/doi/10.1103/PhysRevB.84.100406

[33] J. c. v. Chaloupka, G. Jackeli, and G. Khaliullin, "Zigzag magnetic order in the iridium oxide $\mathrm{na_2iro_3}$," *Phys. Rev. Lett.*, vol. 110, p. 097204, Feb 2013. [Online]. Available: https://link.aps.org/doi/10.1103/PhysRevLett.110.097204

[34] H.-S. Kim, V. S. V., A. Catuneanu, and H.-Y. Kee, "Kitaev magnetism in honeycomb $rucl_3$ with intermediate spin-orbit coupling," *Phys. Rev. B*, vol. 91, p. 241110, Jun 2015. [Online]. Available: https://link.aps.org/doi/10.1103/PhysRevB.91.241110

[35] Z. Alpichshev, F. Mahmood, G. Cao, and N. Gedik, "Confinement-deconfinement transition as an indication of spin-liquid-type behavior in $\mathrm{na_2iro_3}$," *Phys.*

Rev. Lett., vol. 114, p. 017203, Jan 2015. [Online]. Available: https://link.aps.org/doi/10.1103/PhysRevLett.114.017203

[36] S. Hwan Chun, J.-W. Kim, J. Kim, H. Zheng, C. Stoumpos, C. Â. D. Malliakas, J. Â. F. Mitchell, K. Mehlawat, Y. Singh, Y. Choi, T. Gog, A. Al-Zein, M. Â. Sala, M. Krisch, J. Chaloupka, G. Jackeli, G. Khaliullin, and B. J. Kim, "Direct evidence for dominant bond-directional interactions in a honeycomb lattice iridate na2iro3," *Nature Physics*, vol. 11, pp. 462 EP –, May 2015. [Online]. Available: https://doi.org/10.1038/nphys3322

[37] L. J. Sandilands, Y. Tian, K. W. Plumb, Y.-J. Kim, and K. S. Burch, "Scattering continuum and possible fractionalized excitations in $\alpha-\mathrm{rucl}_3$," *Phys. Rev. Lett.*, vol. 114, p. 147201, Apr 2015. [Online]. Available: https://link.aps.org/doi/10.1103/PhysRevLett.114.147201

[38] A. Banerjee, C. A. Bridges, J.-Q. Yan, A. A. Aczel, L. Li, M. B. Stone, G. E. Granroth, M. D. Lumsden, Y. Yiu, J. Knolle, S. Bhattacharjee, D. L. Kovrizhin, R. Moessner, D. A. Tennant, D. G. Mandrus, and S. E. Nagler, "Proximate kitaev quantum spin liquid behaviour in a honeycomb magnet," *Nature Materials*, vol. 15, pp. 733 EP –, Apr 2016, article. [Online]. Available: https://doi.org/10.1038/nmat4604

[39] Y. Singh and P. Gegenwart, "Antiferromagnetic mott insulating state in single crystals of the honeycomb lattice material $\mathrm{na_2iro_3}$," *Phys. Rev. B*, vol. 82, p. 064412, Aug 2010. [Online]. Available: https://link.aps.org/doi/10.1103/PhysRevB.82.064412

[40] Y. Singh, S. Manni, J. Reuther, T. Berlijn, R. Thomale, W. Ku, S. Trebst, and P. Gegenwart, "Relevance of the heisenberg-kitaev model for the honeycomb lattice iridates $A_2\mathrm{iro}_3$," *Phys. Rev. Lett.*, vol. 108, p. 127203, Mar 2012. [Online]. Available: https://link.aps.org/doi/10.1103/PhysRevLett.108.127203

[41] H. Yao and S. A. Kivelson, "Exact chiral spin liquid with non-abelian anyons," *Phys. Rev. Lett.*, vol. 99, p. 247203, Dec 2007. [Online]. Available: https://link.aps.org/doi/10.1103/PhysRevLett.99.247203

[42] S. Yang, D. L. Zhou, and C. P. Sun, "Mosaic spin models with topological order," *Phys. Rev. B*, vol. 76, p. 180404, Nov 2007. [Online]. Available: https://link.aps.org/doi/10.1103/PhysRevB.76.180404

[43] U. F. P. Seifert, J. Gritsch, E. Wagner, D. G. Joshi, W. Brenig, M. Vojta, and K. P. Schmidt, "Bilayer kitaev models: Phase diagrams and novel phases," *Phys. Rev. B*, vol. 98, p. 155101, Oct 2018. [Online]. Available: https://link.aps.org/doi/10.1103/PhysRevB.98.155101

[44] I. Kimchi, J. G. Analytis, and A. Vishwanath, "Three-dimensional quantum spin liquids in models of harmonic-honeycomb iridates and phase diagram in an infinite-d approximation," *Phys. Rev. B*, vol. 90, p. 205126, Nov 2014. [Online]. Available: https://link.aps.org/doi/10.1103/PhysRevB.90.205126

[45] T. Takayama, A. Kato, R. Dinnebier, J. Nuss, H. Kono, L. S. I. Veiga, G. Fabbris, D. Haskel, and H. Takagi, "Hyperhoneycomb iridate $\beta-\mathrm{li_2iro_3}$ as a platform for kitaev magnetism," *Phys. Rev. Lett.*, vol. 114, p. 077202, Feb 2015. [Online]. Available: https://link.aps.org/doi/10.1103/PhysRevLett.114.077202

[46] S. M. Winter, A. A. Tsirlin, M. Daghofer, J. van den Brink, Y. Singh, P. Gegenwart, and R. Valentí, "Models and materials for generalized kitaev magnetism," *Journal of Physics: Condensed Matter*, vol. 29, no. 49, p. 493002, nov 2017. [Online]. Available: https://doi.org/10.1088%2F1361-648x%2Faa8cf5

[47] S. Ryu, "Three-dimensional topological phase on the diamond lattice," *Phys. Rev. B*, vol. 79, p. 075124, Feb 2009. [Online]. Available: https://link.aps.org/doi/10.1103/PhysRevB.79.075124

[48] T. Si and Y. Yu, "Anyonic loops in three-dimensional spin liquid and chiral spin liquid," *Nuclear Physics B*, vol. 803, no. 3, pp. 428 – 449, 2008. [Online]. Available: http://www.sciencedirect.com/science/article/pii/S0550321308003404

[49] K. O'Brien, M. Hermanns, and S. Trebst, "Classification of gapless z_2 spin liquids in three-dimensional kitaev models," *Phys. Rev. B*, vol. 93, p. 085101, Feb 2016. [Online]. Available: https://link.aps.org/doi/10.1103/PhysRevB.93.085101

[50] E. H. Lieb, "Flux phase of the half-filled band," *Phys. Rev. Lett.*, vol. 73, pp. 2158–2161, Oct 1994. [Online]. Available: https://link.aps.org/doi/10.1103/PhysRevLett.73.2158

[51] A. Kitaev, "Fault-tolerant quantum computation by anyons," *Annals of Physics*, vol. 303, no. 1, pp. 2 – 30, 2003. [Online]. Available: http://www.sciencedirect.com/science/article/pii/S0003491602000180

[52] S. Mandal and N. Surendran, "Fermions and nontrivial loop-braiding in a three-dimensional toric code," *Phys. Rev. B*, vol. 90, p. 104424, Sep 2014. [Online]. Available: https://link.aps.org/doi/10.1103/PhysRevB.90.104424

[53] C. Castelnovo and C. Chamon, "Topological order in a three-dimensional toric code at finite temperature," *Phys. Rev. B*, vol. 78, p. 155120, Oct 2008. [Online]. Available: https://link.aps.org/doi/10.1103/PhysRevB.78.155120

[54] S. Iblisdir, D. Pérez-García, M. Aguado, and J. Pachos, "Scaling law for topologically ordered systems at finite temperature," *Phys. Rev. B*, vol. 79, p. 134303, Apr 2009. [Online]. Available: https://link.aps.org/doi/10.1103/PhysRevB.79.134303

[55] S. Iblisdir, D. PÃl'rez-GarcÃ■a, M. Aguado, and J. Pachos, "Thermal states of anyonic systems," *Nuclear Physics B*, vol. 829, no. 3, pp. 401 – 424, 2010. [Online]. Available: http://www.sciencedirect.com/science/article/pii/S055032130900604X

[56] K. Walker and Z. Wang, "(3+1)-tqfts and topological insulators," *Frontiers of Physics*, vol. 7, no. 2, pp. 150–159, Apr 2012. [Online]. Available: https://doi.org/10.1007/s11467-011-0194-z

[57] C. W. von Keyserlingk, F. J. Burnell, and S. H. Simon, "Three-dimensional topological lattice models with surface anyons," *Phys. Rev. B*, vol. 87, p. 045107, Jan 2013. [Online]. Available: https://link.aps.org/doi/10.1103/PhysRevB.87.045107

[58] A. Bullivant and J. K. Pachos, "Entropic manifestations of topological order in three dimensions," *Phys. Rev. B*, vol. 93, p. 125111, Mar 2016. [Online]. Available: https://link.aps.org/doi/10.1103/PhysRevB.93.125111

[59] I. Mondragon-Shem and T. L. Hughes, "Entanglement of a 3d generalization of the kitaev model on the diamond lattice," *Journal of Statistical Mechanics: Theory and Experiment*, vol. 2014, no. 10, p. P10022, 2014. [Online]. Available: http://stacks.iop.org/1742-5468/2014/i=10/a=P10022

[60] H. Yao and X.-L. Qi, "Entanglement entropy and entanglement spectrum of the kitaev model," *Phys. Rev. Lett.*, vol. 105, p. 080501, Aug 2010. [Online]. Available: https://link.aps.org/doi/10.1103/PhysRevLett.105.080501

[61] G. M. Graf and M. Porta, "Bulk-edge correspondence for two-dimensional topological insulators," *Communications in Mathematical Physics*, vol. 324, no. 3, pp. 851–895, Dec 2013. [Online]. Available: https://doi.org/10.1007/s00220-013-1819-6

[62] K. Mullen, B. Uchoa, and D. T. Glatzhofer, "Line of dirac nodes in hyperhoneycomb lattices," *Phys. Rev. Lett.*, vol. 115, p. 026403, Jul 2015. [Online]. Available: https://link.aps.org/doi/10.1103/PhysRevLett.115.026403

[63] M. Ezawa, "Loop-nodal and point-nodal semimetals in three-dimensional honeycomb lattices," *Phys. Rev. Lett.*, vol. 116, p. 127202, Mar 2016. [Online]. Available: https://link.aps.org/doi/10.1103/PhysRevLett.116.127202

[64] A. P. Schnyder and S. Ryu, "Topological phases and surface flat bands in superconductors without inversion symmetry," *Phys. Rev. B*, vol. 84, p. 060504, Aug 2011. [Online]. Available: https://link.aps.org/doi/10.1103/PhysRevB.84.060504

[65] A. A. Burkov, M. D. Hook, and L. Balents, "Topological nodal semimetals," *Phys. Rev. B*, vol. 84, p. 235126, Dec 2011. [Online]. Available: https://link.aps.org/doi/10.1103/PhysRevB.84.235126

[66] K. O'Brien, M. Hermanns, and S. Trebst, "Classification of gapless z_2 liquids in three dimensional kitaev models," *Phys. Rev. B*, vol. 93, p. 085101, Feb 2016. [Online]. Available: https://link.aps.org/doi/10.1103/PhysRevB.93.085101

[67] R. Schaffer, E. K.-H. Lee, Y.-M. Lu, and Y. B. Kim, "Topological spinon semimetals and gapless boundary states in three dimensions," *Phys. Rev. Lett.*, vol. 114, p. 116803, Mar 2015. [Online]. Available: https://link.aps.org/doi/10.1103/PhysRevLett.114.116803

[68] M. Hermanns, K. O'Brien, and S. Trebst, "Weyl spin liquids," *Phys. Rev. Lett.*, vol. 114, p. 157202, Apr 2015. [Online]. Available: https://link.aps.org/doi/10.1103/PhysRevLett.114.157202

[69] D. Wawrzik, D. Lindner, M. Hermanns, and S. Trebst, "Topological semimetals and insulators in three-dimensional honeycomb materials," *Phys. Rev. B*, vol. 98, p. 115114, Sep 2018. [Online]. Available: https://link.aps.org/doi/10.1103/PhysRevB.98.115114

[70] Y. Hasegawa, R. Konno, H. Nakano, and M. Kohmoto, "Zero modes of tight-binding electrons on the honeycomb lattice," *Phys. Rev. B*, vol. 74, p. 033413, Jul 2006. [Online]. Available: https://link.aps.org/doi/10.1103/PhysRevB.74.033413

[71] M. Kohmoto and Y. Hasegawa, "Zero modes and edge states of the honeycomb lattice," *Phys. Rev. B*, vol. 76, p. 205402, Nov 2007. [Online]. Available: https://link.aps.org/doi/10.1103/PhysRevB.76.205402

[72] M. Fujita, K. Wakabayashi, K. Nakada, and K. Kusakabe, "Peculiar localized state at zigzag graphite edge," *Journal of the Physical Society of Japan*, vol. 65, no. 7, pp. 1920–1923, 1996. [Online]. Available: https://doi.org/10.1143/JPSJ.65.1920

[73] M. Thakurathi, K. Sengupta, and D. Sen, "Majorana edge modes in the kitaev model," *Phys. Rev. B*, vol. 89, p. 235434, Jun 2014. [Online]. Available: https://link.aps.org/doi/10.1103/PhysRevB.89.235434

[74] W. P. Su, J. R. Schrieffer, and A. J. Heeger, "Solitons in polyacetylene," *Phys. Rev. Lett.*, vol. 42, pp. 1698–1701, Jun 1979. [Online]. Available: https://link.aps.org/doi/10.1103/PhysRevLett.42.1698

List of Publications

Refereed Journals

1. N. C. Randeep, Naveen Surendran, “Topological entanglement entropy of the three dimension Kitaev model, "Phys.Rev.B, vol. 98, p. 125136, Sep 2018.

2. N. C. Randeep, Naveen Surendran, “Zero-energy Majorana edge modes in three dimensional Kitaev model," Phys.Rev.B, vol. 100, p. 045134, July 2019.

Appendix A

Entanglement entropy of the gauge sector

Our calculation of S_G proceeds as in YQ, and differs from the latter only in that we additionally obtain the explicit dependence on b_0 and b_1.

The full density matrix in the gauge sector is

$$\rho_G = |G(u)\rangle\langle G(u)| = \frac{1}{2^{(N-1)}} \sum_{\tilde{u}\simeq u} |\tilde{u}\rangle\langle\tilde{u}|. \tag{A.1}$$

To compute the reduced density matrix $\rho_{G,A}$ we have to carry out partial trace of ρ_G with respect to the variables in B. But, as pointed out earlier, the variables on the links on the boundary surface between A and B belong to both the regions. In YQ, this difficulty is circumvented by the following procedure.

We can write $|u\rangle = |u_A, u_B, u_p\rangle$, where u_A variables are defined on links entirely in A, u_B on links entirely in B, and u_p on links on the boundary and shared by both A and B. Assuming that the number of boundary links is even, and denoting it by $2L$, we label the corresponding link variables u_p as $u_{a_1,b_1}, u_{a_2,b_2}, \cdots u_{a_{2L},b_{2L}}$, where the sites labeled a_j are in A and those labeled b_j are in B. In terms of Majorana variables, $\hat{u}_{a_j,b_j} = i\gamma_{a_j}^{\alpha_j}\gamma_{b_j}^{\alpha_j}$, where α_j is the link-type of (a_j, b_j). Now define new variables $\hat{w}_{A,n} = i\gamma_{a_{(2n-1)}}^{\alpha_{(2n-1)}}\gamma_{a_{2n}}^{\alpha_{2n}}$ and $\hat{w}_{B,n} = i\gamma_{b_{(2n-1)}}^{\alpha_{(2n-1)}}\gamma_{b_{2n}}^{\alpha_{2n}}$. $\hat{w}_{A,n}$ is defined on the link (a_{2n-1}, a_{2n}), which lies entirely in A; similarly, $\hat{w}_{B,n}$ is defined on (b_{2n-1}, b_{2n}), which lies entirely in B (see Fig. 3.1).

Since $\{u_{ij}\}$ is any gauge-field configuration for which $W_p = 1$ for all plaquettes, we can choose $u_{a_j,b_j} = 1$ for all the boundary links. Then, it is easy to verify that

$$|u_p\rangle = \frac{1}{\sqrt{2^L}} \sum_{w_A=w_B=\pm 1} |w_A, w_B\rangle, \tag{A.2}$$

where w_A and w_B denote the set of eigenvalues of $\hat{w}_{A,n}$ and $\hat{w}_{B,n}$, respectively. Thus,

$$|G(u)\rangle = \frac{1}{\sqrt{2^{N+L+1}}} \sum_g \sum_{w_A=w_B} D_g |u_A, w_A; u_B, w_B\rangle. \tag{A.3}$$

Writing $D_g = X_{g_A} \cdot X_{g_B}$, where g_A is the set of sites in g belonging to A and $X_{g_A} = \prod_{j\in g_A} D_j$. X_{g_B} is similarly defined. Then,

$$\begin{aligned}
\rho_{G,A} = \mathrm{Tr}_B \rho_G &= \frac{1}{2^{N+L+1}} \sum_{g,g'} \sum_{w,w'} X_{g_A} |u_A, w\rangle\langle u_A, w'| X^\dagger_{g'_A} \sum_{u'_B, w''} \langle u'_B, w''| X_{g_B} |u_B, w\rangle \langle u_B, w'| X^\dagger_{g'_B} |u'_B, w''\rangle \\
\rho_{G,A} &= \frac{1}{2^{N+L+1}} \sum_{g,g'} \sum_{w,w'} X_{g_A} |u_A, w\rangle\langle u_A, w'| X^\dagger_{g'_A} \langle u_B, w'| X^\dagger_{g'_B} X_{g_B} |u_B, w\rangle
\end{aligned} \tag{A.4}$$

For $\langle u_B, w'| X^\dagger_{g'_B} X_{g_B} |u_B, w\rangle$ to be nonzero, $w = w'$. Further conditions for its nonvanishing depend on the topology of region B. Let $g_B^{(n)}$, $n = 1, \cdots, n_B$, denote the sites in g_B belonging to the connected component B_n of B. Here n_B is the number of connected components of B. Then the nonvanishing condition becomes: for each n, either ${g'_B}^{(n)} = g_B^{(n)}$, for which $X^\dagger_{{g'_B}^{(n)}} X_{g_B^{(n)}} = 1$, or ${g'_B}^{(n)} = B_n - {g_B}^{(n)}$, in which case $X^\dagger_{{g'_B}^{(n)}} X_{{g_B}^{(n)}} = X_{B_n}$ (here $X_{B_n} \equiv X_{g=B_n}$). In both the cases $\langle u_B, w'| X^\dagger_{g'_B} X_{g_B} |u_B, w\rangle = 1$. Let N_A and N_B be the number of sites in A and B, respectively (with $N_A + N_B = N$). Then,

$$\rho_{G,A} = \frac{2^{n_B}}{2^{N_A+L+1}} \sum_{g_A, g'_A, w} X_{g_A} |u_A, w\rangle\langle u_A, w| X^\dagger_{g'_A}. \tag{A.5}$$

Next we calculate $\rho^2_{G,A}$ and show that it is proportional to $\rho_{G,A}$.

$$\rho^2_{G,A} = \left(\frac{2^{n_B}}{2^{N_A+L+1}}\right)^2 \sum_{\substack{g_A, g'_A, w \\ \tilde{g}_A, \tilde{g}'_A, w'}} X_{g_A} |u_A, w\rangle\langle u_A, w| X^\dagger_{g'_A} X_{\tilde{g}_A} |u_A, w'\rangle\langle u_A, w'| X^\dagger_{\tilde{g}'_A}. \tag{A.6}$$

As before, $\langle u_A, w| X^\dagger_{g'_A} X_{\tilde{g}_A} |u_A, w'\rangle$ is nonzero only when $w = w'$ and, for each connected component A_n in A, either ${g'_A}^{(n)} = g_A^{(n)}$, or ${g'_A}^{(n)} = A_n - {g_A}^{(n)}$, (here ${g_A}^{(n)}$ denotes the sites in g_A belonging to A_n). Then

$$\rho^2_{G,A} = \left(\frac{2^{n_B}}{2^{N_A+L+1}}\right)^2 \times 2^{N_A+n_A} \sum_{g_A, g'_A, w} X_{g_A} |u_A, w\rangle\langle u_A, w| X^\dagger_{g'_A}, \tag{A.7}$$

where n_A is the number of connected components in A. Thus,

$$\rho_{G,A}^2 = 2^{n_A+n_B-L-1}\rho_{G,A}. \tag{A.8}$$

From the properties of density matrix it then immediately follows that the entanglement entropy $S_G = L\ln 2 - (n_A + n_B - 1)\ln 2$. But $n_A+n_B-1 = b_0$, the number of connected components (zeroth Betti number) of the boundary surface between A and B, and we have

$$S_G = L\ln 2 - b_0 \ln 2. \tag{A.9}$$

Appendix B

Existence condition for armchair edge modes

The solution for armchair edge modes given by Eq. (4.37) exists when $|x_{\pm}| < 1$, which is possible only when $|J_x| > |J_y|$. By Eq. (4.33)]

$$|x_{\pm}| = \sqrt{\frac{|J_y|}{t|J_x|}} \left| \left(1 \pm \sqrt{1 + te^{i\theta}}\right) \right| \tag{B.1}$$

Here we have put $J_z = 1$; θ is the phase of $-(\alpha J_1^*)^2$ and

$$t = \left|4J_1^2 J_x J_y\right|. \tag{B.2}$$

Let

$$1 + te^{i\theta} = \rho e^{i\phi}. \tag{B.3}$$

Then

$$\left| \left(1 \pm \sqrt{1 - te^{i\theta}}\right) \right|^2 = (1 + \rho \pm 2\sqrt{\rho}\cos(\phi/2)) \tag{B.4}$$

Using Eqs. (B.3),

$$|x_{\pm}|^2 = \frac{|J_y|}{t|J_x|} \left\{ 1 + \left(1 + t^2 + 2t\cos\theta\right)^{\frac{1}{2}} \pm \sqrt{2} \Big[\left(1 + t^2 + 2t\cos\theta\right)^{\frac{1}{2}} + (1 + t\cos\theta) \Big]^{\frac{1}{2}} \right\} \tag{B.5}$$

Evidently, $|x_+| > |x_-|$, therefore, for the edge modes to exist $|x_+| < 1$ is sufficient. Furthermore, since $x_+ x_- = J_y/J_x$, $|x_+| < 1$ can be satisfied only when $|J_x| > |J_y|$.

For a given t, let x_+^{max} and x_+^{min} be the maximum and minimum values for $|x_+|$, respec-

tively. Then

$$(x_+^{max})^2 = \frac{|J_y|}{t|J_x|}\left\{1 + (1+t) + 2(1+t)^{\frac{1}{2}}\right\}, \tag{B.6}$$

$$(x_+^{min})^2 = \frac{|J_y|}{t|J_x|}\left\{1 + (1-t) + 2(1-t)^{\frac{1}{2}}\right\}. \tag{B.7}$$

For edge modes to exist for all $\mathbf{k}$, $x_+^{max} < 1$. This leads to $|J_x| - |J_y| > 1$, which corresponds to Region 2 in the phase diagram. For edge modes to exist for at least some $\mathbf{k}$, $x_+^{min} < 1$, which implies $|J_x| + |J_y| > 1$. This corresponds to the region in the gapless phase (shaded area in Fig. 4.1) in which $|J_x| > |J_y|$.

In a similar way we can show that the edge modes given by Eq. (4.38) exist for all $\mathbf{k}$ in Region 3 and at least for some $\mathbf{k}$ in the gapless phase, provided $|J_y| > |J_x|$.